15555   MEDIUM-GRAINED OLIVINE-NORMATIVE   ST. 9A   9614.0 g
              MARE BASALT

INTRODUCTION: 15555 ("Great Scott") is both the largest and the most intensively studied of the Apollo 15 rocks. It is a medium-grained olivine basalt, with a few percent small vugs (Fig. 1). It is probably very close to a liquid composition, i.e., it contains few, if any, accumulated crystals. It crystallized ~3.3 b.y. ago. Unlike other nearby rocks, 15555 was not dust-coated. It is generally tough, but many exterior chips fell off during earth transit and many of these pieces are friable. It is sub-rounded and blocky (Figs. 1,2), with many zap pits.

15555 was collected about 12 meters north of the rim of Hadley Rille, with no fresh craters in its immediate vicinity, and from an area with fewer rocks exposed than at the Rille edge.
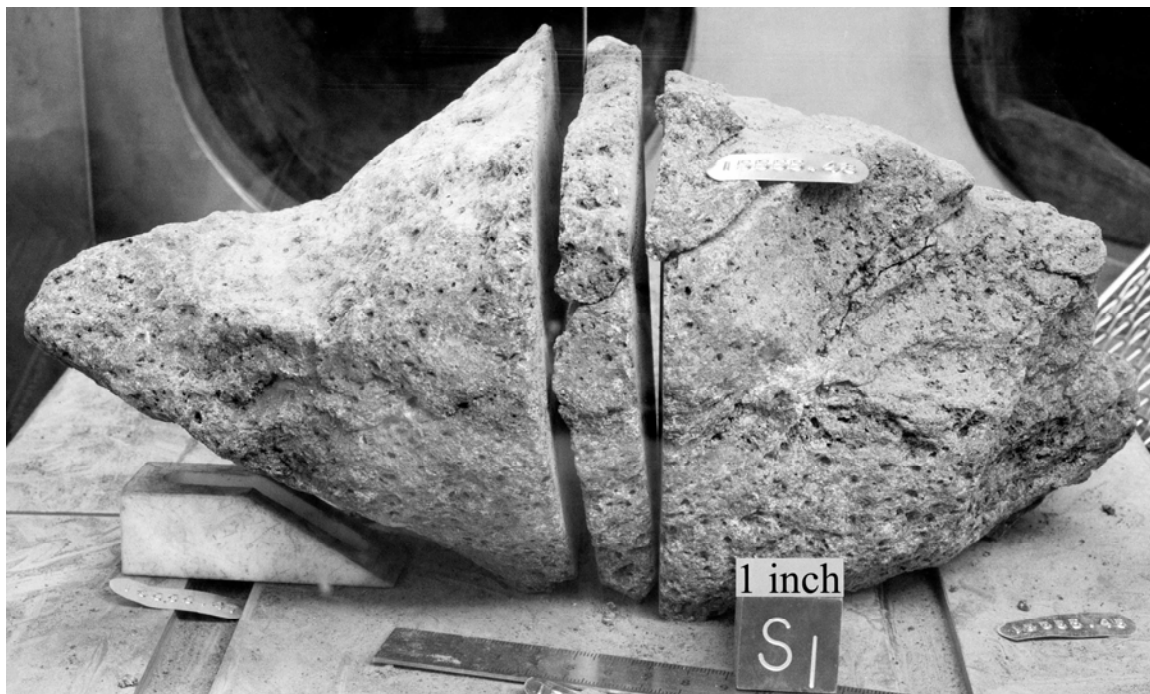

Figure 1. Saw cutting of 15555,0. S-71-57105

PETROLOGY: 15555 is among the coarsest of the olivine basalts. Macroscopically it is dark brownish gray, with red-brown and honey-brown pyroxenes, translucent plagioclases, and yellowish olivines clearly visible. Vugs are conspicuous and evenly distributed (Fig. 3); they contain euhedral crystals. The thin sections are generally equigranular but pigeonite and olivine have frequently been described as phenocrysts.

The plagioclases ophitically enclose smaller olivines and augite (Fig. 4). Plagioclases are up to ~4 mm long, pigeonites commonly 2 mm or more long and twinned, and olivines commonly about 1 mm. All these minerals, and the opaque oxides, are zoned. There is very little mesostasis.
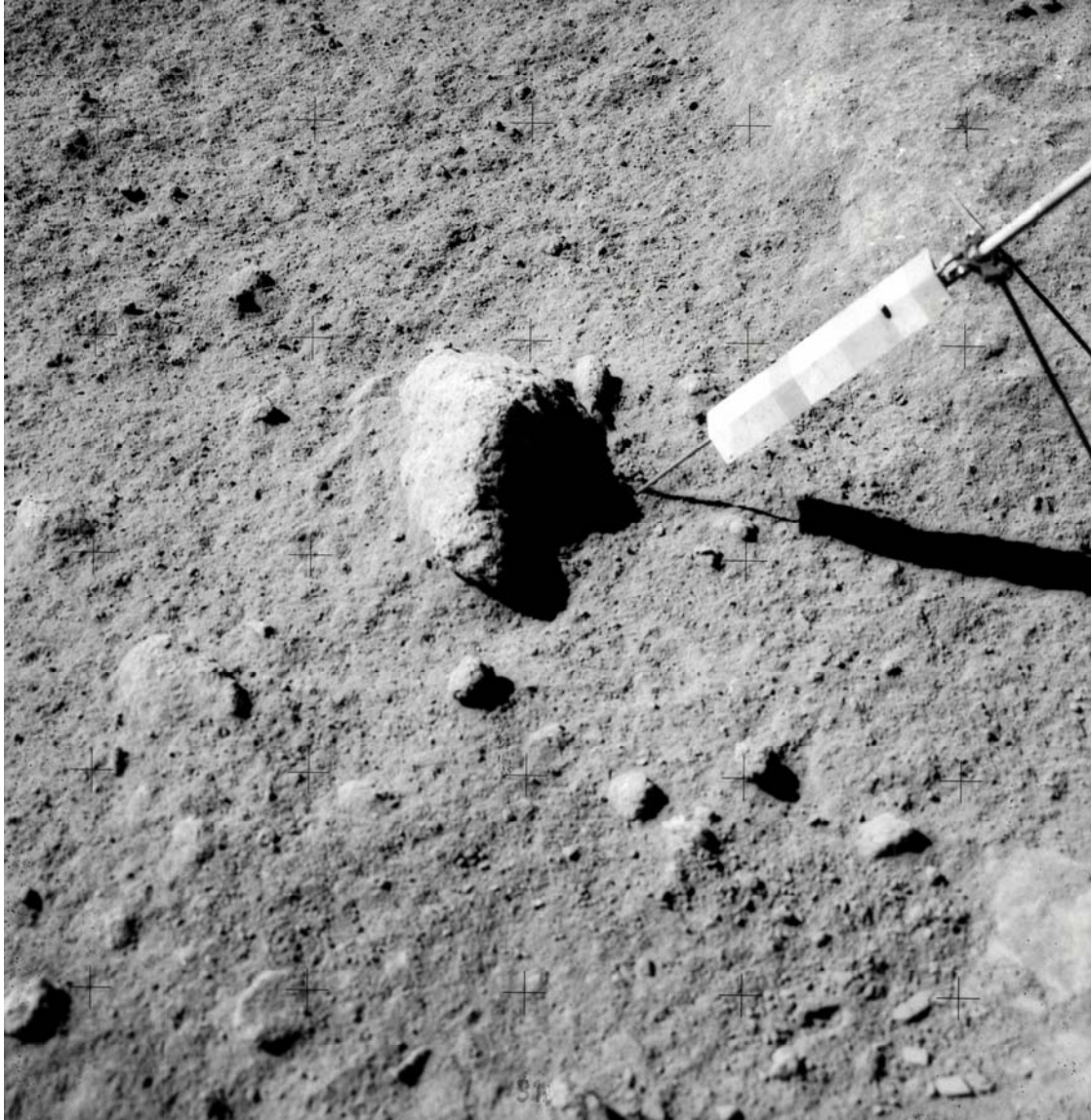

Figure 2. Presampling photograph. AS-15-82-11164

Descriptions of the petrography and silicate mineralogy and chemistry (microprobe data) were given by Heuer et al. (1972), Longhi et al. (1972), Papike et al. (1972), Bence and Papike (1972), Brown et al. (1972a,b), Chappell et al. (1972), Mason et al. (1972), Boyd (1972), Bell and Mao (1972a,b), Michel-Levy and Johann (1973), Nord et al. (1973), Crawford (1973), Dalton and Hollister (1974), Walker et al. (1977), and L. Taylor et al. (1977). These reports differ more in emphasis than substance. Published modes (Table 1) are reasonably consistent given the coarse grain size.

TABLE 15555-1. Published modes of 15555 thin sections

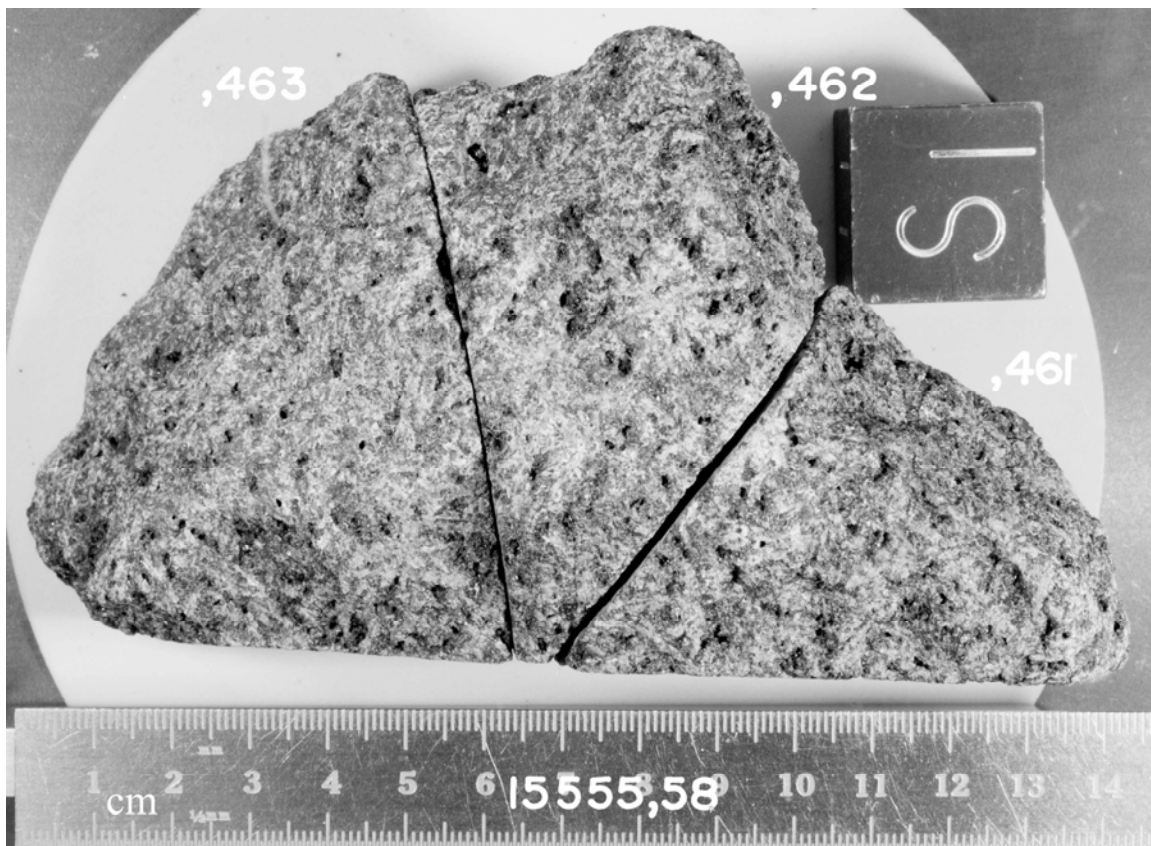| OL	PX	PL	GL+SIL	OPQ	REFERENCE
12.1	52.4	30.4	2.3	2.7	Longhi et al. (1972)
20	40	35	5		Heuer et al. (1972) Nord et al. (1973)
15	55	26	1.5	3	A15 Lunar Sample Information Catalog (1971)

Figure 3. Close-up showing vuggy nature. S-74-31408

According to Bell and Mao (1972a,b) olivines are of two varieties. One has large grains (0.5-1.55 mm) with rounded edges, and includes several complex and reversely zoned specimens (Fo_{40} cores to Fo_{60} rims), although others are quite uniform. The second variety is of smaller grains (10-100 μm) which are euhedral, less strongly zoned (Fo_{60-50}), and ophitically included in plagioclases. Other reports have similar or consistent descriptions (Longhi et al. 1972, Bence and Papike 1972, Mason et al. 1972, Heuer et al. 1972, Chappell et al. 1972, and Dalton and Hollister 1974) but with slightly different compositional ranges. Chappell et al. (1972) stated that the most magnesian olivine is Fo_{61}; Longhi et al. (1972) reported a range of Fo_{71-59}; Walker et al. (1977) showed zoning profiles extending that range down Fo_{40}. Dalton and Hollister (1974) reported a wide range from Fo_{67-29} for the larger olivines, and divide the small olivines into two textural types: euhedral/subhedral in plagioclases are Fo_{49-16}; anhedral in pyroxenes are Fo_{63-48}. L. Taylor et al. (1977) showed a compositional zoning profile from Fo_{62-15} over a distance of 300 μm. Brown et al. (1972b) reported one olivine zoned continuously from Fo_{50} to Fo_8. Heuer et al. (1972) found the olivines to be devoid of substructure other than a moderate density of dislocations produced during cooling. Olivines are significant for the estimation of cooling rates for 15555 (below).

Pyroxenes are composite and described by Heuer et al. (1972), Longhi et al. (1972), Papike et al. (1972), Brown et al. (1972b), Bence and Papike (1972), Mason et al. (1972), Nord et al. (1972), Dalton and Hollister (1974), Boyd (1972), Walker et al. (1977), Michel-Levy and Johann (1973), and Chappell et al. (1972). Quadrilateral diagrams are shown in Figure 5. Boyd (1972) described the zoning in most detail: pigeonite cores have sector-zoned mantles of more Ca-rich pyroxene (see Fig. 5). Pyroxferroite did not form; instead ferroaugite with fayalite + cristobalite appears. Mason et al. (1972) described some complex and in some places oscillatory zoning in pyroxenes (Fig. 6). Bence and Papike also showed and tabulated detailed analytical profiles. The most iron-rich pyroxenes are the ferroaugites which occur as small, euhedral grains enclosed in plagioclases. The trends in pyroxene minor element chemistry, in particular discussed by Bence and Papike (1972), Dalton and Hollister (1974) and Walker et al. (1972), are of significance in establishing the crystallization sequence of minerals in 15555 (below).

Heuer et al. (1972) and Nord et al. (1973) described exsolution features (revealed with HVTEM techniques) as well as anti-phase domains. In the cores, the pyroxene consists of 300 Å pigeonites and 80 Å augite plates; away from the core the augite lamellae are coarser and have a different orientation. Papike et al. (1972) reported some x-ray diffraction data for pyroxenes, and concluded that 15555 cooled a little more slowly than the isochemical sample 15016.
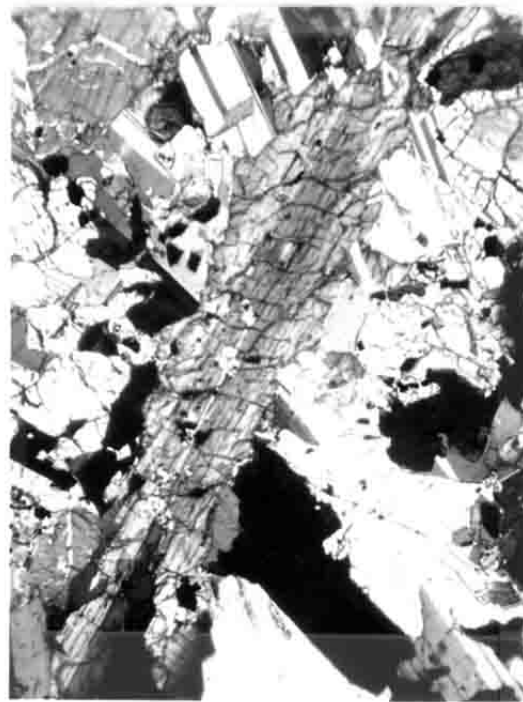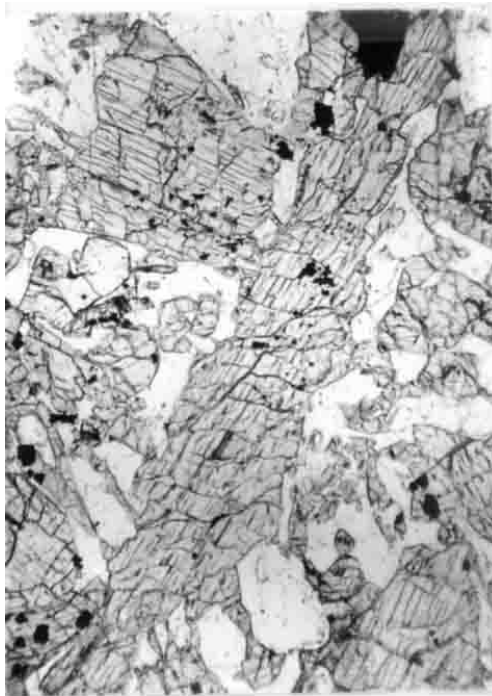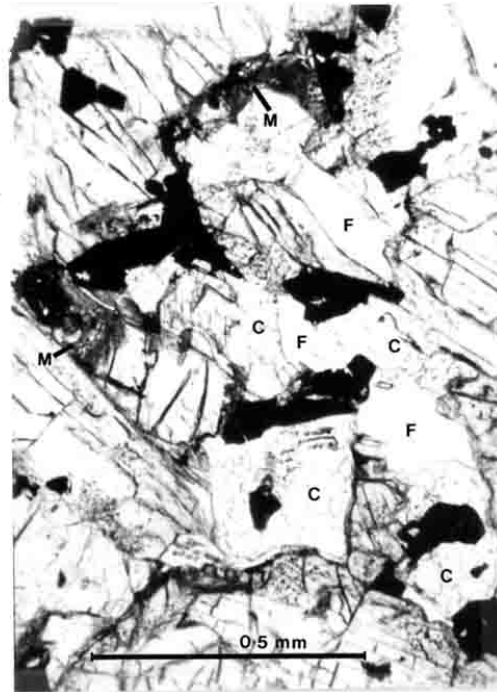
Figure 4. Photomicrographs of 15555. (a) Whole thin section ,257, partly crossed polarizers; (b) 15555,257, crossed polarizers, width 3mm, showing zoned pyroxene; (c) as (b) transmitted light, and showing euhedral spinels; (d) interstitial area of 15555,170, transmitted light. M = mesostasis, F = feldspar, C = cristobalite.
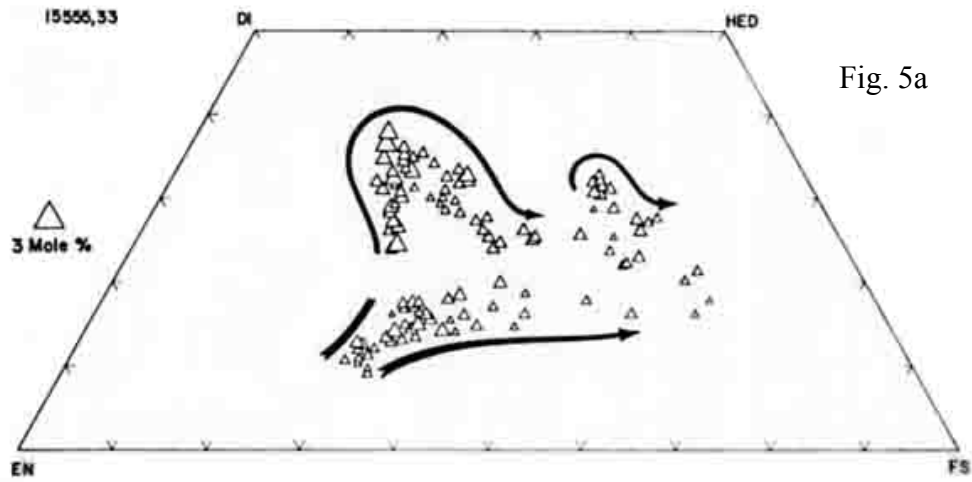
Fig. 5a

PYROXENES SELECTED AT RANDOM
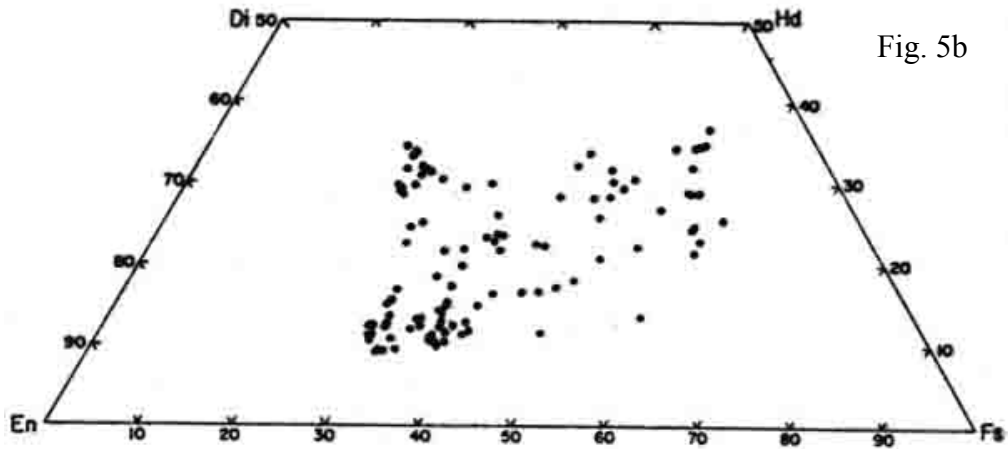
Fig. 5b

SCAN ⊥ (0I0)   IO MICROMETER STEPS

Fig. 5c

SCAN ⊥ (100)   IO MICROMETER STEPS

Di 50   50 Hd   Fig. 5d
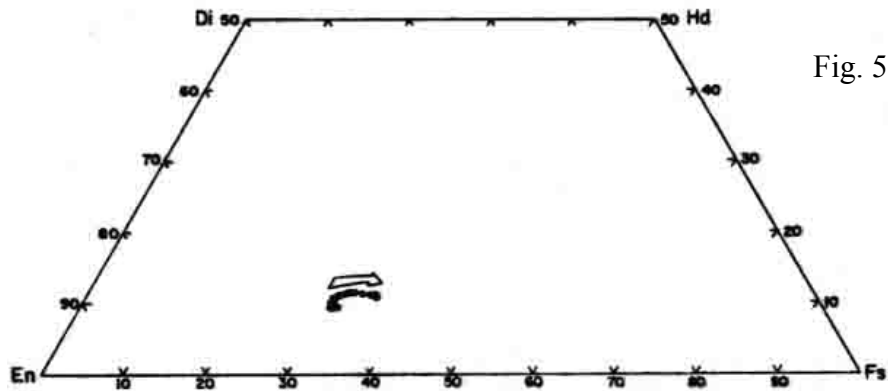
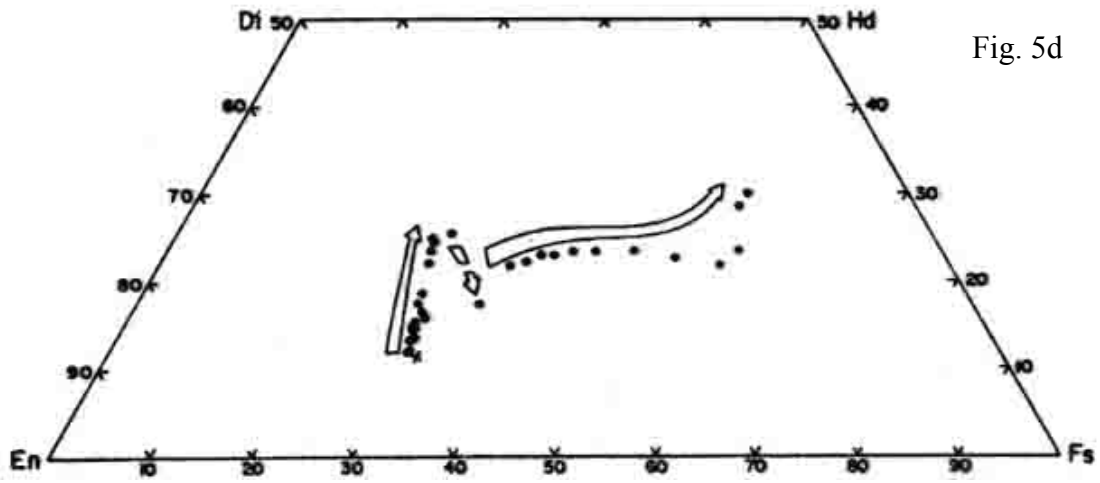SCAN ⊥ (IIO)   IO MICROMETER STEPS

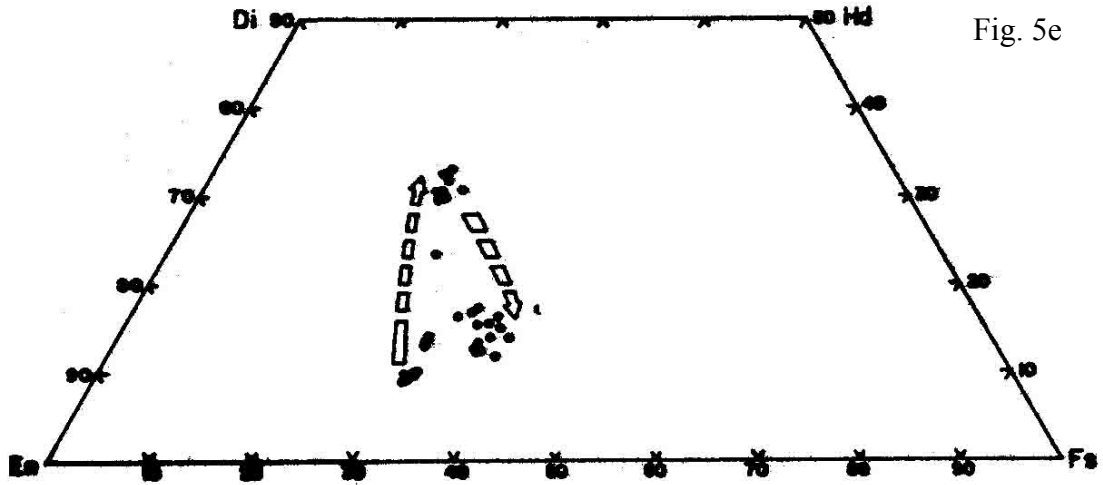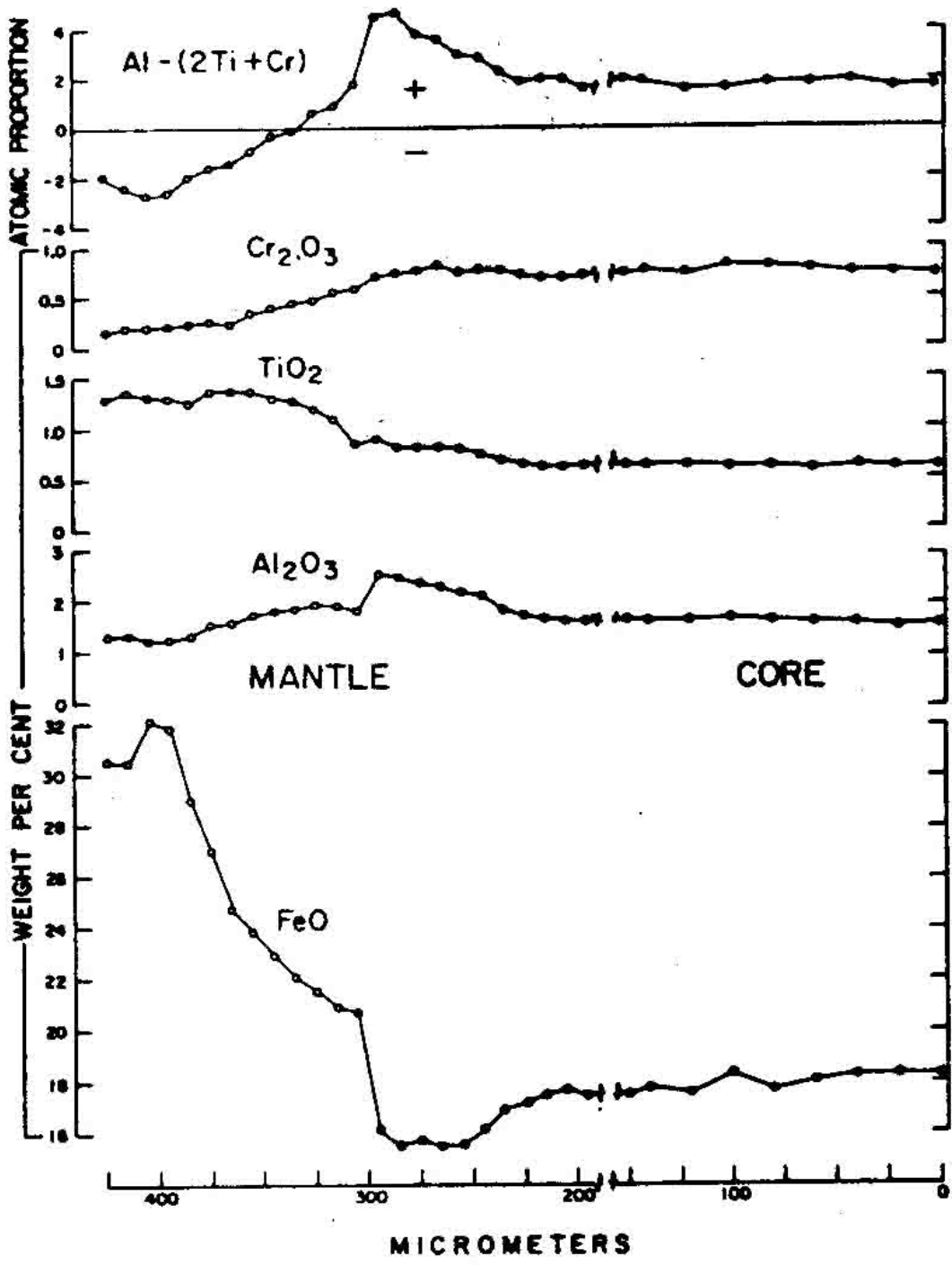Di 90   90 Hd   Fig. 5e

Fig. 5f

Figure 5. Pyroxene quadrilaterals and zoning profiles.
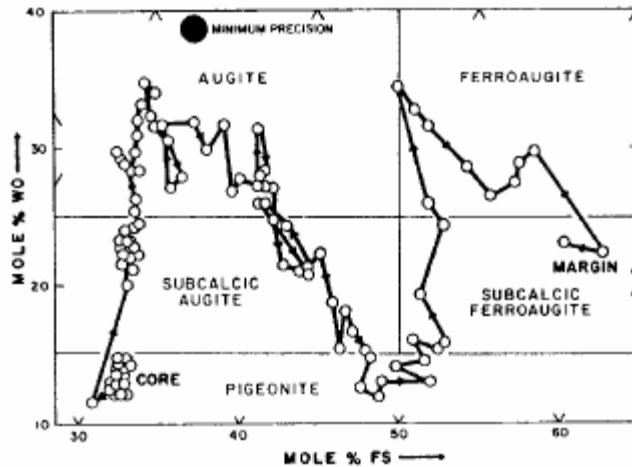(a) Bence and Papike (1972); (b) to (f) Boyd (1972).

Figure 6. Pyroxene zoning profile (Mason, 1972).

Plagioclases, which ophitically enclose small olivines and augites, are more or less anhedral and are zoned normally. Longhi et al. (1972) reported a range of An_{94-78}, with homogeneous cores (An_{94-91}; Fe/Mg = 0.5). The rims have the strong zoning, An_{91-78}; Fe/Mg = 0.6 to 0.9. Longhi et al. (1976) plotted Fe/Fe+Mg v. Ca/Ca+Na+K for natural cores, mantles, and rims, and noted that iron increases as calcium decreases. Crawford (1973) reported microprobe scans and analyses: the early plagioclase is a lath, zoned but not hollow, which grows into a more irregular shape. FeO/FeO+MgO of the core is 0.62, of the margins 0.88. The plagioclases deviate from ideal compositions in the manner common for lunar plagioclases. Meyer et al. (1974) made ion-probe traverses across plagioclase for the analyses of Mg, Ca, St, K, and Ba. Sr, Ba, and K concentrations increase towards the grain boundaries. Czank et al. (1973) found weak, diffuse c-reflections in plagioclases, and Wenk and Wild (1973) briefly reported on optical properties derived from universal stage work. Heuer et al. (1972) reported on small (900 Å) b-type domains in plagioclase, and found no unambiguous evidence of plagioclase exsolution. Wenk et al. (1973) also reported small b-type anti-phase domains, and Nord et al. (1973) found that the anti-phase domains have morphologies correlated with composition. They also reported weak exsolution.

Detailed studies of the oxide phases, with microprobe analyses, were presented by Haggerty (1971, 1972a,b,c,d), Dalton and Hollister (1974), and El Goresy et al. (1976). The oxides are spinels (chromite-ulvospinel series) and ilmenites. 15555 is among the few basalts which have spinels whose compositions span the entire normal-inverse series (Fig. 7, 8). However, intermediate compositions are not as common as others, and discontinuous mantling does occur. Corroded and rounded chromite cores as inclusions in later members of the series suggests a reaction relationship between Ti-chromite and liquid (El Goresy et al. (1976). Idiomorphic Ti-chromites, optically unzoned but chemically zoned, are included in olivines. Haggerty (1972c) concluded that Ti^{3+} and Cr^{2+} can be present in only very small abundances, if at all. Ilmenite occurs as discrete grains and as lamellae in reduced spinel; Haggerty (1971, 1972a) in particular discussed

subsolidus reduction of chromite to intergrowths of ulvospinel, ilmenite, and Fe-metal. About 10% of the chromite has been so reduced. Blank et al. (1982) analyzed opaque oxides for the trace elements Zr and Nb using a proton microprobe. These elements are of very low abundance in primary chromite (<5 ppm) but higher in chromian ulvospinels (Zr 250-2000 ppm; Nb 20-300 ppm). The oxide compositional changes have been considered important indicators of changing liquid compositions resulting from crystallization of silicate phases, hence of value in assessing the crystallization sequence of 15555 (below) (see especially Dalton and Hollister 1974, and El Goresy et al. (1976).

Brown et al. (1972b) and Peckett et al. (1972) reported the discovery of a Zr-Ti-Fe mineral with high concentrations of Y and REEs ("Phase Y") in the 15555 mesostasis, and provided a microprobe analysis. Roedder and Weiblen (1972) reported on inclusions, including melt inclusions, in mineral phases, particularly olivine and ilmenite, with microprobe analyses. The olivines contain numerous tiny silicate "melt" inclusions, now assemblages of ilmenite, glass, immiscible sulfide, and shrinkage bubbles. Roedder and Weiblen (1972) also reported on high-Fe and high-Si immiscible melt inclusions in plagioclase and cristobalite.

Crystallization sequence: The textural, mineral chemical and zoning, and experimental (see EXPERIMENTAL PETROLOGY, below) data have been utilized to infer details of the crystallization sequence of 15555. From Ti/Al zoning in pyroxenes, Longhi et al. (1972) suggested that 45% crystallization had taken place before plagioclase started to crystallize, 90% before ilmenite. The low-pressure experimental sequence of ol→px→plag matches that inferred for the rock itself. Dalton and Hollister (1974) used the microprobe analyses of host and inclusion mineral pairs to deduce the crystallization sequence. The reversal from increasing to decreasing Ca and Al in pyroxenes is interpreted by these authors to coincide with the incoming of plagioclase under supersaturation, in agreement with Longhi et al. (1972) and others. They could not find evidence to indicate whether olivine, chromite, or pigeonite crystallized first, but all precede plagioclase. They did conclude that there was no significant settling of mineral phases, with the possible exception of chromite. El Goresy et al. (1976) concluded that the chromites probably preceded pigeonite, either during or preceding olivine. Walker et al. (1977), using experimental data extensively to deduce the relationship between the rock composition and the original liquid from which it crystallized, inferred, like Dalton and Hollister (1977) that there was little, if any, accumulation.

Apart from cooling history studies, other mineralogical studies are dominated by those elucidating valence states of cations, e.g., Mossbauer studies. Weeks (1972) found the intensity of Fe^{3+} spectra from plagioclase to be greater than in Apollo 14 rocks, and believed the Fe^{3+} not to result from radiation damage; the study did not detect Ti^{3+}. Burns et al. (1972) measured polarized absorption spectra on single crystals of pyroxene to identify Fe and Ti valences; Ti^{3+} bands were not observed. A spectra taken for olivine (Burns et al., 1973) found the expected Cr^{3+} bands, but lead to the conclusion that the inference of Cr^{2+} which had been made for lunar olivines was not convincing. Bell and Mao (1972c) analyzed an olivine (Fo_{50}) and found polarized bands attributable to Fe^{3+}. Huffman et al. (1972, 1974, 1975) made Mossbauer analyses and magnetic studies:

98.5% of Fe is in silicates (77.6% in px, 20.9% in ol) with 1.3% in ilmenite. Fe metal (0.055 wt.%) was not detected in the Mossbauer study. Virtually all of the Fe is Fe^{2+}, and totals 18.7%. Abu-Eid et al. (1973) found Fe^{3+} to be less than the detectability level of 1%.

Simmons et al. (1975) illustrated a possible natural stress-induced crack of tectonic rather than shock origin, as well as radial cracks most probably resulting from thermal expansion. A healed crack is marked by a bubble chain (glass inclusions).
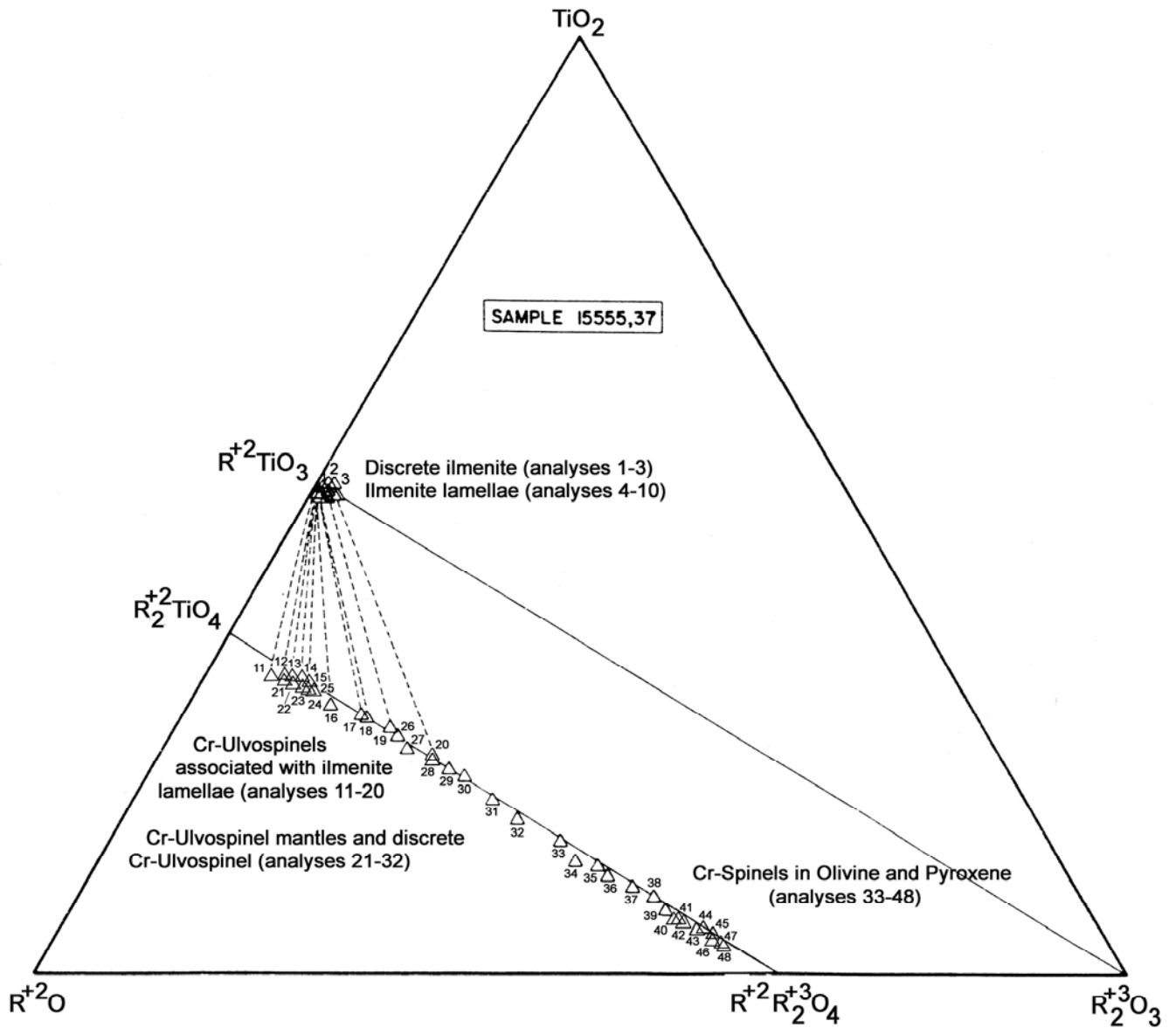
Fig. 7a
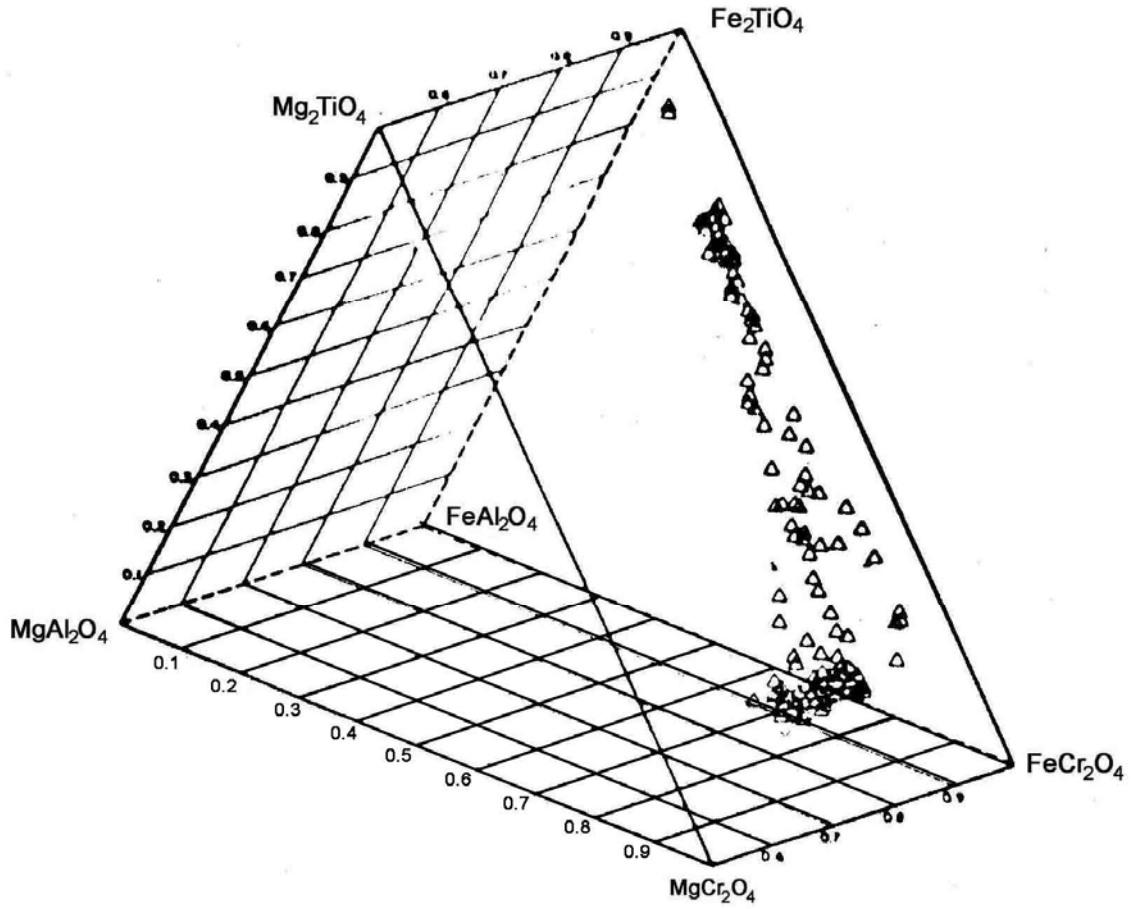
Fig. 7b
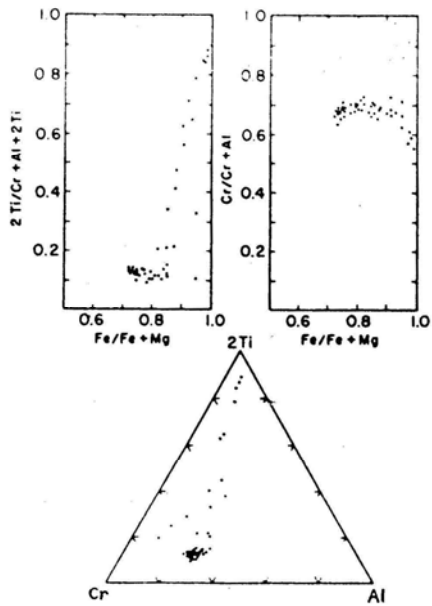
Fig. 7c
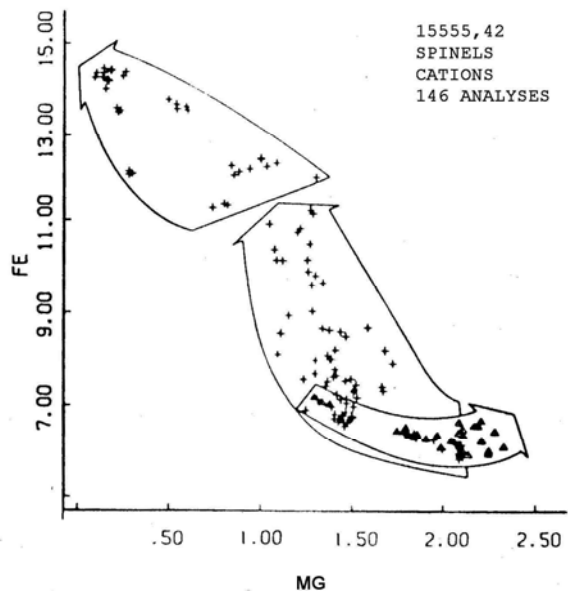
Fig. 7d
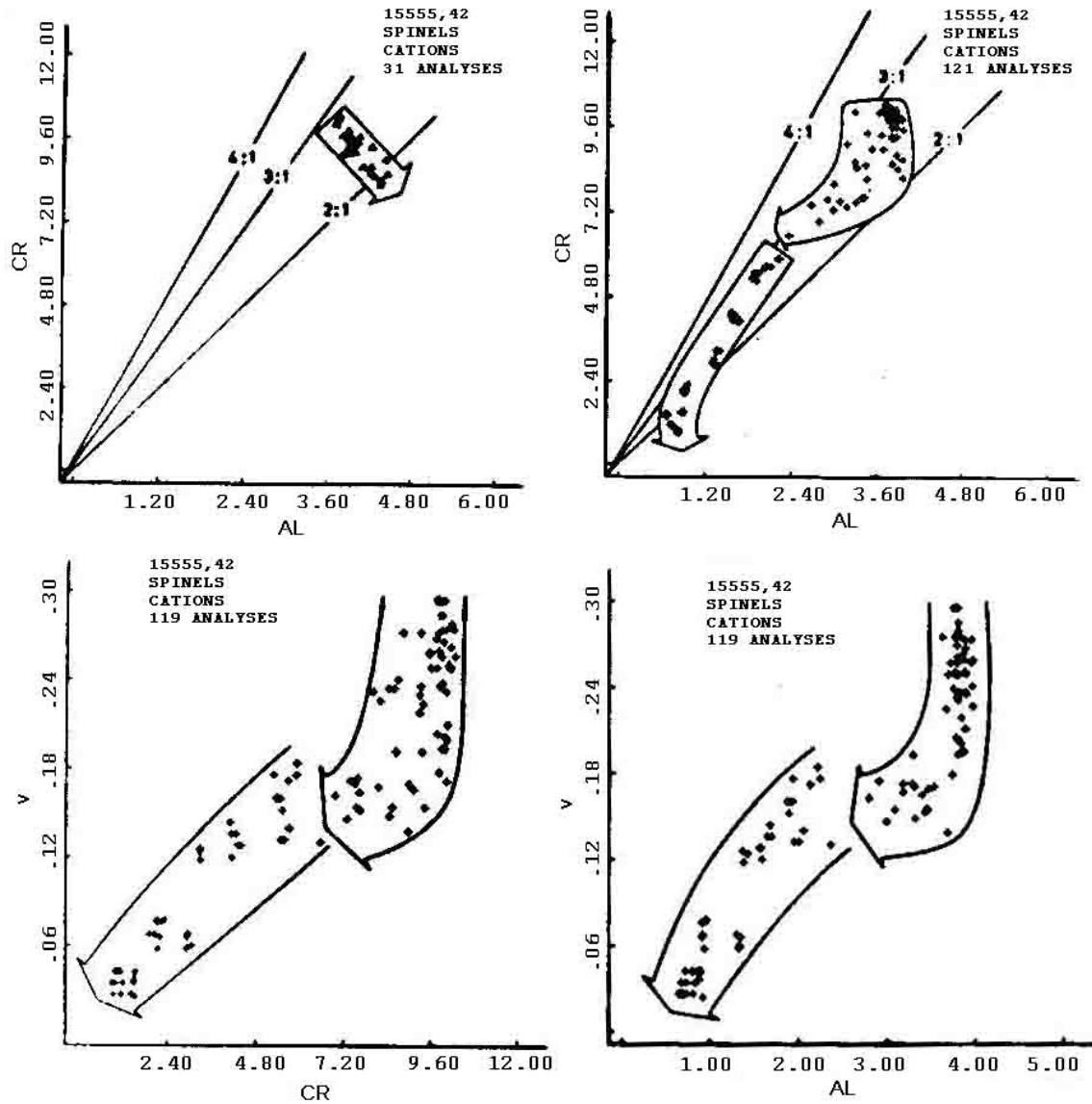
Fig. 7e

Figure 7. Spinel compositions. (a) Haggerty (1971); (b) Haggerty (1972c);
(c) Dalton and Hollister (1974); (d) and (e) El Goresy et al. (1976).

Cooling history: Estimates of the cooling rate(s) for 15555 have been made utilizing mineral compositional data and experimental data. 15555 is too coarse-grained for direct analog with the products of dynamic crystallization experiments (Walker et al. 1977), other than to give maximum rates. Pyroxene cores in the experimental products are similar to natural ones, and implies that there was little supercooling at pyroxene entry (Walker et al., 1977); pyroxenes maintained surface equilibrium (cores not erased), but rims depart from equilibrium trends. Ti/Al in experimental samples approaches 1/2 rather than 1/4 as in natural samples, thus 15555 had delayed nucleation of plagioclase

followed by its rapid growth. Olivine natural cores are Fo_{71}, cf. Fo_{73} in equilibrium experiments, hence olivine is not accumulative and was reequilibrated during cooling (however, O'Hara and Humphries, 1977, cautioned against "over-interpretation" of small differences of Mg/Fe in experiments because of iron-loss problems). Olivine major-element zoning profiles, compared with modeled diffusion and equilibration, suggest ~4°C/day cooling during early olivine crystallization (Walker et al., 1977), thus 15555 is from a location a few meters from the edge of a flow which took a few months to cool. Taylor et al. (1977), modeling Fe-Mg diffusion and olivine zoning profiles, deduced ~5°C/day (minimum rate), and Onorato et al. (1978) improved on these diffusion models by including diffusion in the liquid. Bianco and Taylor (1977) found that olivines in 2°C/hr. cooling experiments had morphologies similar to those in 15555 except that they were internally skeletal. From the olivine nucleation density they estimated a cooling rate of 0.5 to 1.0°C/hr. at the beginning of olivine crystallization (assuming that the erupted melt was olivine-free). Cukierman et al. (1973) reported data on the kinetics of crystallization of a glass of 15555 composition, noting that it does not form glass easily.

EXPERIMENTAL PETROLOGY: Several equilibrium experimental crystallization studies have been conducted on a 15555 composition, at low and high pressures (Humphries et al., 1972; Longhi et al., 1972; Kesson, 1975, 1977; and Walker et al., 1977). Longhi et al. (1978) included 15555 (natural rock powder) in experiments specifically to determine the distribution of Fe and Mg between olivine and basaltic liquids, and Bianco and Taylor (1977) used a Ca-depleted 15555-iike composition for isothermal and constant cooling rate experiments. The problems of iron-loss to the containers are widely recognized and discussed in detail by O'Hara and Humphries (1977) and Walker et al. (1977).
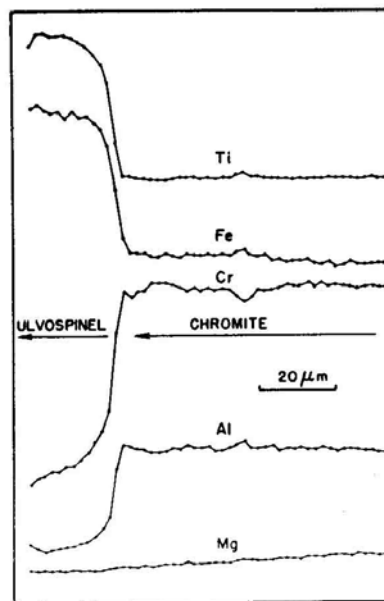
Figure 8. Spinel zoning profile
(Dalton and Hollister, 1974).

The experimental data are depicted in Figure 9. Some of the differences result from iron-loss according to the capsules and conditions used, as discussed by Walker et al. (1977) and O'Hara and Humphries (1977). The data are similar except that spinel appears earlier in the Humphries et al. (1972) diagram, and except for the Mg/Fe of mafic phases. Walker et al. (1972) noted that the olivine and pyroxene natural core compositions are close to those in the equilibrium experiments, so that little crystal accumulation took place and 15555 is close to a liquid composition. This is in disagreement with O'Hara et al. (1975), and the evidence is discussed extensively by Walker et al. (1977). The high pressure experiments show similar multiple saturation points with olivine and low-Ca pyroxene without spinel. The difference of several kilobars between the Kesson (1975, 1977) and the Longhi et al. (1972) and Walker et al. (1977) multiple saturation points may be a calibration difference as much as a result of different conditions and capsules. Assuming multiple saturation, twelve kb indicates a 240 km depth for the source liquid of 15555, deeper if olivine separation took place during ascent (Kesson, 1975).

Figure 9. Experimental phase petrology.
(a) and (b) Longhi et al. (1972); (c) Humphries et al. (1972).

TABLE 15555-2. Bulk rock chemical analyses

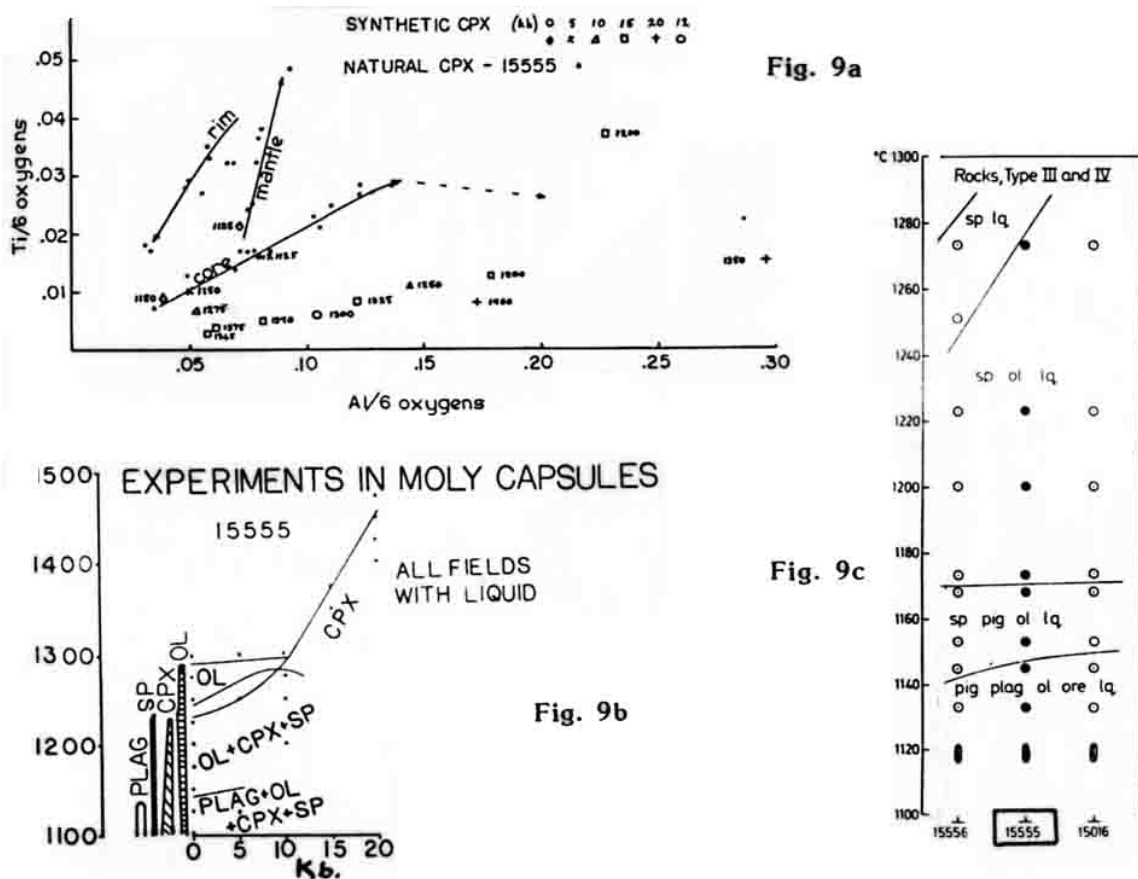|	,225	,157	,149	,59	,27	,25	,148	,134	,153	,8
Wt % SiO_2	45.86	44.75			43.21		43.0	45.2	44.22	44.24
TiO_2	2.40	2.07	2.04	2.05	1.73		2.8	2.3	2.36	2.26
Al_2O_3	8.29	8.67	8.41	9.24	10.32		8.5	9.3	7.54	8.48
FeO	23.45	23.40	22.2	21.4	20.16		21.8;22.4;23.0	21.0	24.24	22.47
MgO	11.55	11.48			11.20		10.2	11.9	11.11	11.19
CaO	9.24	9.14	10.4	9.9	9.96				9.18	9.45
Na_2O	0.34	0.24	0.28	0.28	0.35		0.39	0.39	0.29	0.24
K_2O	0.09	0.05			0.05				0.04	0.03
P_2O_5		0.05			0.05				0.06	0.06
(ppm) Sc			38.4	43.1	40		38;38;38			
V		145	244	266	240					
Cr	4700	4200;4500	4820	4720	4500		3620;3530;3570		5200	
Mn		2300	2300	2310	1900		2100	2000	2250	2250
Co		66	61.8	50.3	87		54;58;52			
Ni		70	90	50	96					42
Rb		<5	0.75	0.84	1.1	0.65				0.6
Sr		83	84	88	93					92
Y		47			23					23
Zr		60			58		124;130;124			76
Nb					17					4.3
Hf			2.1	3.1	<20		3.12;3.20;3.26			
Ba		30	47	59	30					
Th			0.30	0.40	<100					
U			0.14	0.21	<500					
Pb			<2							
La			3.5	4.8						
Ce			10	18	<100					
Pr										
Nd					<100					
Sm			3.2	4.0						
Eu			0.75	1.00			0.93;1.1;1.3			
Gd										
Tb			0.51	0.77			0.92;0.93;—			
Dy			3.2	4.4						
Ho			0.78	0.91						
Er			2.7	3.3						
Tm										
Yb			1.64	1.59	4.2					
Lu			0.43	0.39						
Li		7			5.5					
Be										
B		3								
C										
N										
S										700
F										
Cl										
Br					6000					
Cu		17	6.6	7.1	13a					
Zn			1.3	1.2		0.78				
(ppb) I										
At										
Ga		3000	2900	3700	4600					
Ge						8.5				
As			<50	<50						
Se			85	106		156				
Mo										
Tc										
Ru										
Rh										
Pd										
Ag			<7	<7	200	1.0				
Cd						2.1				
In			2	<2		0.55				
Sn										
Sb						0.067				
Te						3.4				
Cs			26	32	30					
Ta			290	400			1500;1400;1400			
W			1200	430						
Re						0.0013				
Os										
Ir			<0.1	<0.1		0.006				
Pt										
Au			0.48	0.85		0.139c				
Hg										
Tl						0.20				
Bi						0.089				
	(1)	(2)	(3)	(4)	(5)	(6)	(7)	(8)	(9)	(10)

TABLE 15555-2 Continued

		.20	.18	.13	.16	.13	.33	A	B			.15
Wt %	SiO2		45.0	44.75	43.82							
	TiO2	2.25	1.60	2.05	2.63							
	Al2O3	8.5	9.37	9.01	7.45							
	FeO	23.2	21.18	21.68	24.58							
	MgO		12.22	11.39	10.96							
	CaO		9.25	9.62	9.22		8.4h					
	Na2O	0.2655	0.26	0.27	0.24							
	K2O		0.03;0.0276	0.04	0.04		0.0421			0.0646		
	P2O5		0.007;0.066	0.06	0.07							
(ppm)	Sc	40										
	V											
	Cr	4100	3300	4100	4200							
	Mn		2000	2300	2500							
	Co	50										
	Ni											
	Rb		0.445	0.54	0.76	0.63				0.874		0.700
	Sr		84.4	92.2	90.7	89.9				92.0		85.32
	Y			18								
	Zr		57.3	69								
	Nb			5								
	Hf	2.2										
	Ba		32.2									41.61
	Th							0.4596	0.4296		0.3095	
	U							0.1264	0.1173		0.0850	
	Pb							0.209	0.191		0.1388	
	La	5.4										
	Ce		8.06									
	Pr											
	Nd		6.26									
	Sm	3.5	2.09									
	Eu	1.18	0.688									
	Gd		2.90									
	Tb	0.7										
	Dy		3.27									
	Ho											
	Er		1.70									
	Tm											
	Yb	2.1	1.45									
	Lu	0.37										
	Li		6.36									
	Be											
	B											
	C											
	N											
	S			400	600							
	F											
	Cl											
	Br											
	Cu											
	Zn											
	I											
	Ar											
	Ga			2700								
	Ge											
	As											
	Se											
	Mo											
	Tc											
	Ru											
	Rh											
	Pd											
	Ag											
	Cd											
	In											
	Sn											
	Sb											
	Te											
	Cs											
	Ta											
	W											
	Re											
	Os											
	Ir											
	Pt											
	Au											
	Hg											
	Tl											
	Bi											
		(11)	(12)	(13)	(14)	(15)	(16)	(17)	(17)	(17)	(18)	(19)

TABLE 15555-2 Continued

		(19)	(20)	(21)	(22)	(23)	(24)	(25)	(26)	(27)	(28)	(29)	(30)	(31)	(32)
		,12			,144	,144	,143				,135	,135	,479	,81	,195
Wt %	SiO_2														
	TiO_2														
	Al_2O_3														
	FeO														
	MgO														
	CaO														
	Na_2O														
	K_2O		0.0376	0.0390											
	P_2O_5														
(ppm)	Sc														
	V														
	Cr						3540;3830;4390								
	Mn														
	Co														
	Ni														
	Rb	0.538	0.675	0.62k											
	Sr	74.11	86.9j	91.0j											
	Y														
	Zr														
	Nb														
	Hf														2.001/1.96
	Ba														
	Th														
	U														
	Pb														
	La														
	Ce														
	Pr														
	Nd						11.85m								7.518
	Sm							3.784							2.520
	Eu														
	Gd														
	Tb														
	Dy														
	Ho														
	Er														
	Tm														
	Yb														
	Lu														.255/.250
	Li														
	Be						0.28								
	B														
	C				7.3	7.7					12		7.7n		
	N										<2		<0.8		
	S							855	726		650	580	>12.9		
	F														
	Cl														
	Br														
	Cu														
	Zn													980	
(ppb)	I														
	At														
	Ga														
	Ge														
	As														
	Se														
	Mo														
	Tc														
	Ru														
	Rh														
	Pd														
	Ag														
	Cd														
	In														
	Sn														
	Sb														
	Te														
	Cs														
	Ta														
	W														
	Re														
	Os														
	Ir														
	Pt														
	Au														
	Hg														
	Tl														
	Bi													0.25	

References to Table 15555-2.

References and methods:

(1)   Longhi et al. (1972); EMP/FB
(2)   Mason et al. (1972); Gen. sil.
(3)(4) Brunfelt et al. (1972); INAA
(5)   Christian et al. (1972), Cuttitta et
      al. (1973b); Combined, XRF, etc.
(6)   Morgan et al. (1972d), Ganapathy et al.
      (1973); RNAA
(7)   Janghorbani et al. (1973), except Zr,
      Hf from Chyi and Ehmann (1973); RNAA
(8)   Janghorbani et al. (1973); RNAA
(9)   Maxwell et al. (1972); Combined
(10) Rhodes and Hubbard (1973), PET (1972);
      XRF
(11) Fruchter et al. (1973); INAA
(12) Schnetzler et al. (1972), Nava (1974e);
      AAS, Col, ID
(13) Chappell and Green (1973), Compston et
      al. (1972f); XRF
(14) Chappell and Green (1973), Chappell et
      al. (1972); XRF, ID
(15) Compston et al. (1972); ID
(16) Husain et al. (1972a), Husain (1974);
      MS
(17) Tatsumoto et al. (1972); ID, MS
(18) Tera and Wasserburg (1974); ID, MS
(19) Murthy et al. (1972); ID, MS
(20) Mark et al. (1973); ID, MS
(21) Birck et al. (1975); ID, MS
(22) Friedman et al. (19721); Combustion
(23) Friedman et al. (19721); Pyrolysis
(24) Eisentraut et al. (1972); GC
(25) Lugmair (1975); ID, MS
(26) Gibson et al. (1975); Combustion
(27) Gibson et al. (1975); Hydrolysis
(28) Kaplan et al. (1976); Combustion
(29) Kaplan et al. (1976); Hydrolysis
(30) Desmarais et al. (1978); Combustion
(31) Allen et al. (1973); INAA
(32) Unruh et al. (1984); ID/MS

Other Notes:

(a)   Listed erroneously as 0.13 ppm in
      Cuttitta et al. (1972).
(b)   Also list very high upper limits for
      several trace elements.
(c)   Listed by Ganapathy et al. (1973) as
      "doubtful value": contamination.
(d)   Units not stated, but ppb except Zn, Rb
      ppm. Te not listed.
(e)   Majors only.
(f)   Rb, Sr only.
(g)   K only.
(h)   From 39Ar abundance.
(i)   From 37Ar abundance.
(j)   Calc. from 86Sr and isotopic ratios.
(k)   Calc. from 87Rb and isotopic ratios.
(l)   Also provide H abundances.
(m)   Calc. from 144Nd and isotopic ratios.
(n)   5.6 indigenous, 2.1 terrestrial
      contamination.

CHEMISTRY: 15555 has been widely allocated for chemical analyses, with resulting duplicate data for many elements (Table 2). There is also data on mineral separates (Table 3). Apart from noting the conformity with other Apollo 15 olivine basalts, most papers do not specifically discuss the chemistry other than to relate discrepancies between analyses to the coarse grain size of the sample. Most of the data suggest that 15555 is a fairly average Al5 olivine-normative mare basalt, Christian et al. (1972) analyzed for ferric iron but found none, reporting 0.00%. Rare-earth element data are illustrated in Figure 10 and indicate probable sampling biases and systematic errors.

STABLE ISOTOPES: Published data are listed in Table 4. Data for ^{204}Pb (generally considered stable on account of its long half-life) published by Allen et al. (1973b) are lower from those previously reported by them (Allen et al., 1973a), but the change is not noted or discussed. In general the stable isotope data received no specific discussion. The isotopic compositions distinguish 15555 from regolith, as expected. According to Friedman et al. (1972), the hydrogen is probably a mixture of spallationogenic hydrogen with that left over after melting and partial outgassing.

TABLE 15555-3. Chemical analyses of mineral separates

	,149 Plag	,149 Lt.Cpx	,149 Dk.Cpx	,149 Oliv	Plag	Px
Wt % SiO2						
TiO2	0.20	1.19	1.27	<0.17		
Al2O3	33.09	4.61	2.31	1.06		
FeO	0.6	13.8	27.9	39.3		
MgO	<1.7	13.1	6.8	24.9		
CaO	25.5	8.5	14.4	1.7		
Na2O	0.97	0.15	0.03	0.12		
K2O					0.0433	0.0126
P2O5						
(ppm) Sc	0.5	65.9	71.0	10.0		
V	53	212	115	82		
Cr	8	531	196	192		
Mn	7.5	2169	3024	2842		
Co	1.2	32.0	42.2	103.5		
Ni	<10	148	<10	54		
Rb	<0.9	5.1	<0.9	1.3	0.131	0.204
Sr	310	<10	16	<10	282	26.1
Y						
Zr						45
Nb						
Hf	<0.9	0.1	3.2	<0.9		
Ba	18	<15	60	25	27.1	12.2
Th	<0.20	<0.20	0.29	<0.20		
U	<0.10	<0.10	<0.10	<0.10		
Pb						
La	<0.5	1.0	6.3	1.8		
Ce					1.25	3.14
Pr						
Nd					0.87	2.99
Sm	0.21	1.84	6.12	0.82	0.27	1.19
Eu	1.80	<0.40	0.86	<0.50	1.84	0.27
Gd					0.34	1.88
Tb	0.02	0.55	1.20	0.19		
Dy	0.1	3.1	6.2	1.1	0.39	2.29
Ho						
Er						1.27
Tm						
Yb	0.1	1.6	3.6	0.53	0.14	1.04
Lu						
Li					11.3	4.97
Be						
B						
C						
N						
S						
F						
Cl						
Br						
Cu						
Zn						
(ppb) I						
At						
Ga						
Ge						
As						
Se						
Mo						
Tc						
Ru						
Rh						
Pd						
Ag						
Cd						
In						
Sn						
Sb						
Te						
Cs	100	490	<100	1050		
Ta	<100	<100	130	<100		
W						
Re						
Os						
Ir						
Pt						
Au						
Hg						
Tl						
Bi						
	(1)	(1)	(1)	(1)	(2)	(2)

References and methods:

(1) Brunfelt et al. (1973a); INAA
(2) Schnetzler et al. (1972); AAS, Col, ID

GEOCHRONOLOGY AND RADIOGENIC ISOTOPES: Several different groups have reported Rb-Sr isotopic data and results (Table 5; Figure 11). Two analytically significant discrepancies are the old age determined by Chappell et al. (1972), and the low initial $^{87}Sr/^{86}Sr$ determined by Murthy et al. (1972a, b). These discrepancies are discussed by Papanastassiou and Wasserburg (1973) whose opinion is that the Chappell et al. (1972) data is affected by serious analytical difficulties. They also measured $^{87}Sr/^{86}Sr$ in four plagioclase separates to test the suggestion of Murthy et al. (1972a) that differences in initial $^{87}Sr/^{86}Sr$ result from original variations within the rock, but concluded that the rock had uniform initial ratios throughout its volume. Thus 15555 has a Rb-Sr age close to 3.32 b.y. and an initial $^{87}Sr/^{86}Sr$ ratio similar to other Apollo 15 olivine basalts. T_{BABI} model ages calculated by Nyquist (1977) for much of the data are quite varied.
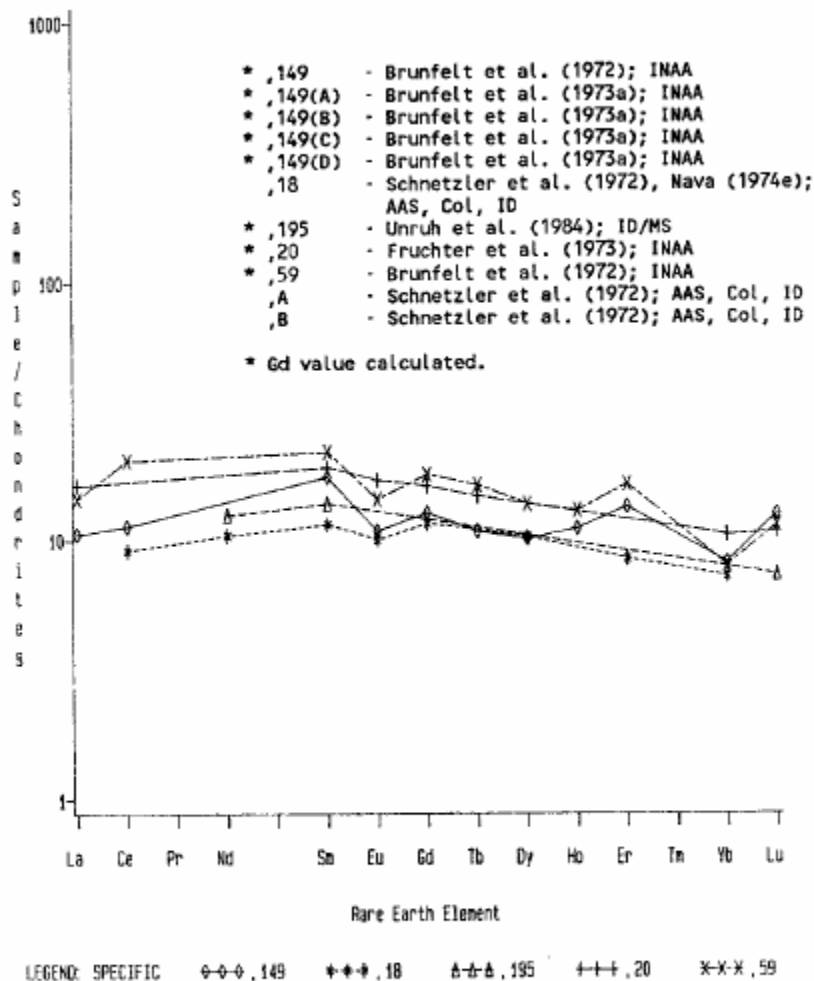
Fig. 10a
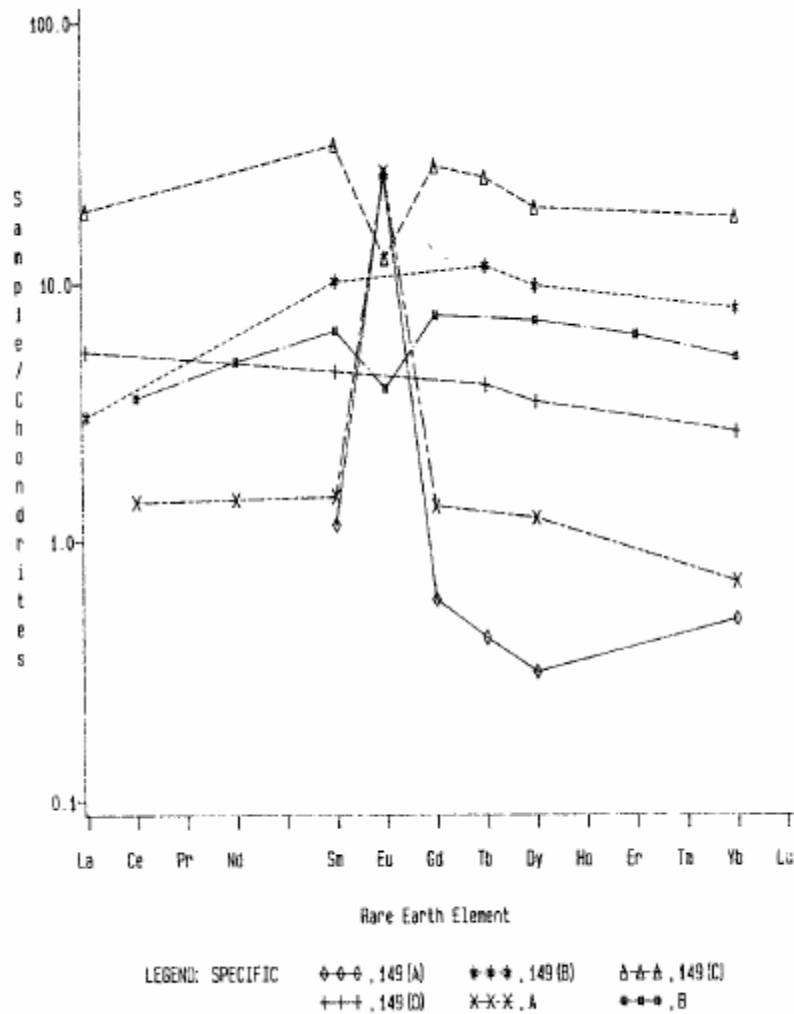
Figure 10. (a) Rare earths in bulk rock 15555;
(b) rare earths in mineral separates from 15555.

^{40}Ar-^{39}Ar age determinations are consistent with those of Rb-Sr data (Table 6; Figure 12), averaging about 3.32 b.y., as is a K-Ar age of 3.31 ± 0.07 b.y. determined by Murthy et al. (1972b). However, Husain et al. (1972b) determined a lower K-Ar age of 2.87 b.y. (uncertainty not stated), and Lightner and Marti (1972) also determined a K-Ar age of 2.8 b.y. Analysts tend to agree that 15555 has lost about 20% of its radiogenic ^{40}Ar, leading to K-Ar ages lower than Ar-Ar ages. Podosek et al. (1972) concluded that 60% of the potassium is in minor phases, in quintessence, making quantitative evaluation difficult; the "real" age is best given by the plagioclase determination which in any case gives the best plateau. The Podosek et al. (1972) release data were also presented and discussed by Turner et al. (1972).

TABLE 15555-4. Stable isotopic data for 15555

D	^{13}C	^{34}S	^{204}Pb	EXTRACTION	REFERENCE
-90	-24			Pyrolysis	Friedman et al. (1972)
	-27.5			Combustion	Friedman et al. (1972)
	-14			Combustion	Kaplan et al. (1976)
		+0.7		Combustion	Kaplan et al. (1976)
		+0.8		Hydrolysis	Kaplan et al. (1976)
	-27.8			Combustion	DesMarais (1978)
			<0.2ppb	Leach, Leach residues	Allen et al. (1973b)

TABLE 15555-5. Summary of Rb-Sr isotopic results for 15555 whole rock

REFERENCE	INT. ISOCH. AGE (b.y.)	INITIAL $^{82}Sr/^{86}Sr$	MEASURED $^{87}Sr/^{86}Sr$	MEASURED $^{87}Rb/^{86}Sr$
Compston et al. (1972)			0.70051±10	0.0203
Tatsumoto et al. (1972)			0.70062	
Chappell et al. (1972)	3.54±0.13	0.69936±8	0.70042±5 0.70062±10	0.0220 0.0226
Murthy et al. (1972a,b)	3.30±0.08	0.69906±4	0.70009±6 0.70005±5	0.02375 0.02102
Mark et al. (1973)			0.70032±8	0.0218a
Wasserburg and Papanastassiou (1971)	3.32±0.06[b]	0.69934[c]±5		
Cliff et al. (1972)	3.34d			
Birck et al. (1975)	3.34±0.09	0.69927	0.70046±15	0.0262

Notes:

(a) erroneously reported as 0.218
(b) uncertainty revised down to 0.04 by Papanastassiou and Wasserburg
(1973) from recalculations using different tracer $^{87}Sr/^{84}Sr$
(c) value reported as 0.69930 in Papanastassiou and Wasserburg (1973)
(d) no isotopic data reported

Fig. 11a
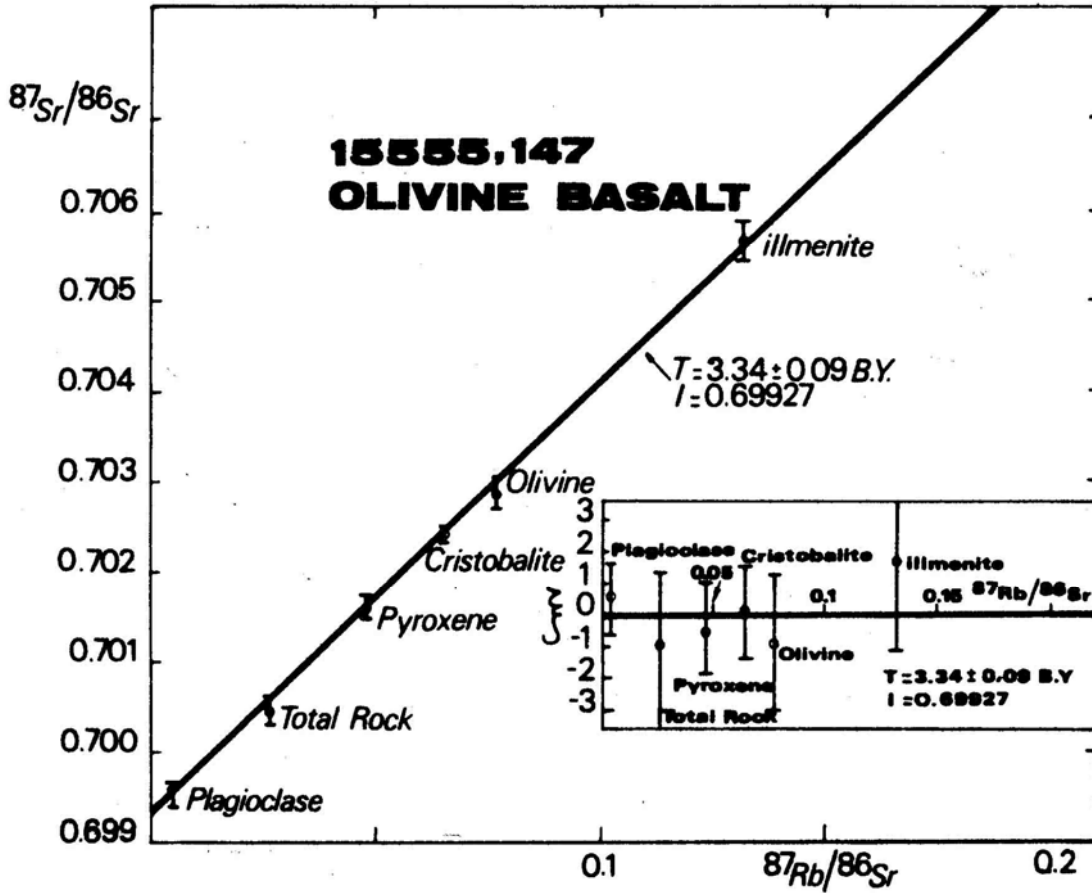
$^{87}Sr/^{86}Sr$, $^{87}Rb/^{86}Sr$ diagram for Apollo 15555,147 rock. The inset corresponds to ξ, $^{87}Rb/^{87}Sr$ diagram.

$$\xi = \left\{ \frac{(^{87}Sr/^{86}Sr) \text{ measured} - (^{87}Sr/^{86}Sr) \text{ best fit line}}{(^{87}Sr/^{86}Sr) \text{ best fit line}} \right\} \times 1000$$

I is the $(^{87}Sr/^{86}Sr)$ initial ratio.

Fig. 11b

Fig. 11c

Model 4.5 × 10⁹ years

3.54 ± 0.13 × 10⁹ years
0.69936 ∓ 8
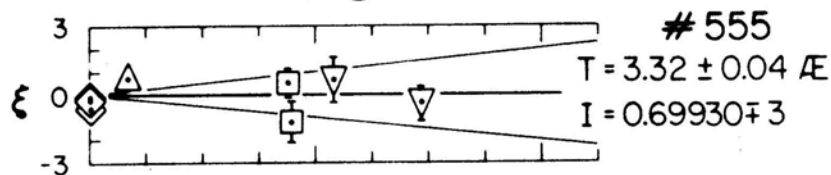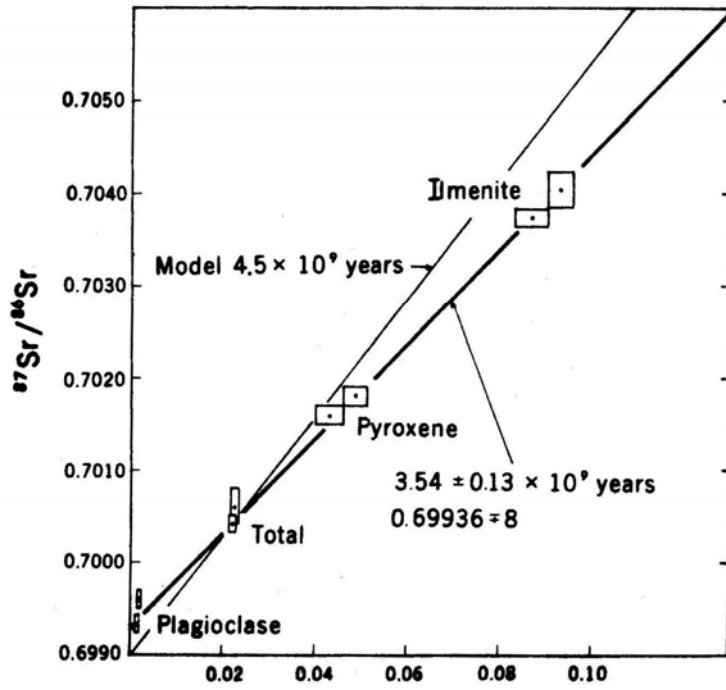
Fig. 11d
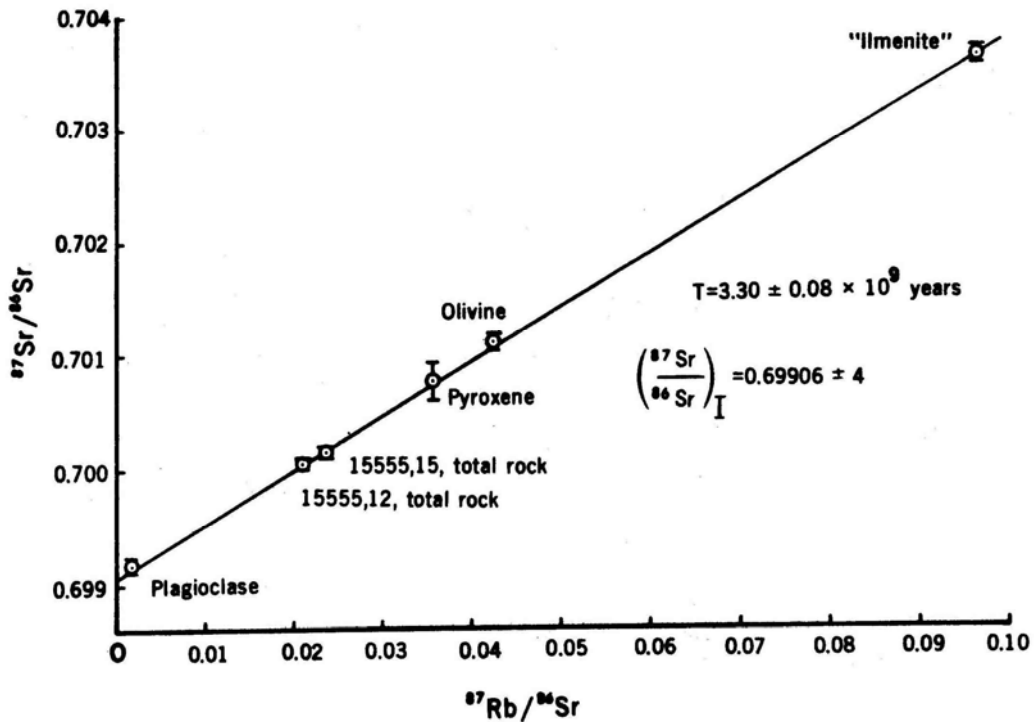
Figure 11. Rb-Sr internal isochrons. (a) Birck et al. (1975); (b) Papanastassiou and Wasserburg (1973); (c) Chappell et al. (1972); (d) Murthy et al. (1972a).
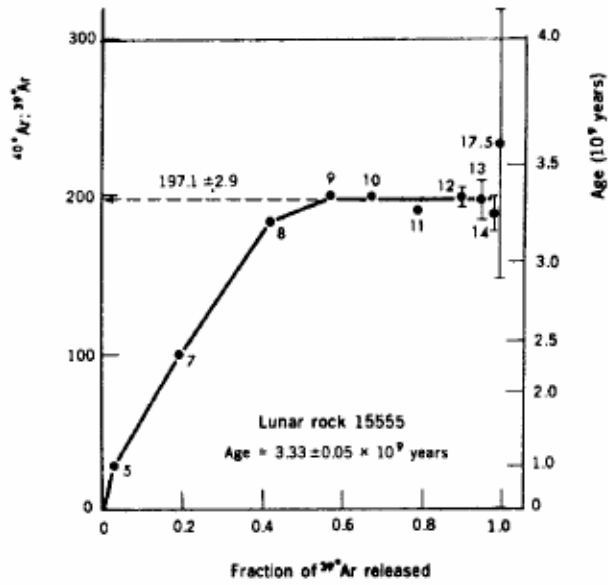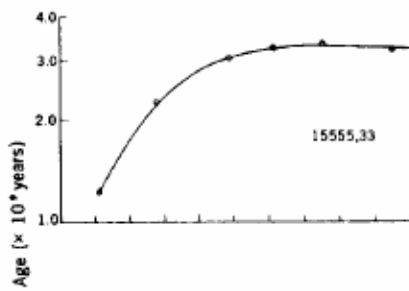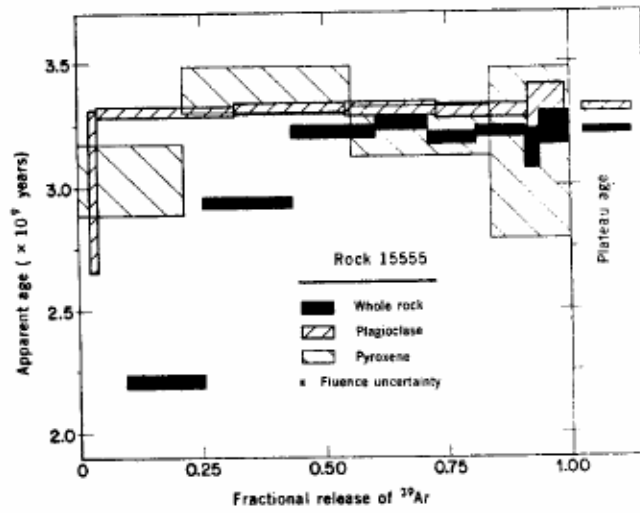
Figure 12. Ar release diagrams. (a) Alexander et al. (1972);
(b) Podosek et al. (1972); (c) Husain et al. (1972a

TABLE 15555-6. Summary of ^{40}Ar-^{39}Ar gas retention ages for 15555

REFERENCE	MATERIAL	AGE (b.y.)
Podosek et al. (1972)	WR	3.219 ± .025
Podosek et al. (1972)	PL.	3.308 ± .025
Podosek et al. (1972)	PL.	3.32 ± .05
Podosek et al. (1972)	PX.	3.328 ± .09
Alexander et al. (1972)	WR	3.33 ± .05
York et al. (1972a)	WR, 2 dups.	3.31 ± .06
Husain et al. (1972a)	WR	3.28 ± .06

TABLE 15555-7a. Sm/Nd whole rock isotopic data for 15555,82 (Lugair, 1975)

^{147}Sm/^{144}Nd	(^{143}Nd/^{144}Nd)s	(^{143}Nd/^{144}Nd)
0.1991 ± 2	0.512887 ± 34	0.512863 ± 13

s = from spiked sample

TABLE 15555-7b. Sm/Nd and Lu/Hf whole-rock isotopic data for 15555,195
(Unruh et al., 1984)

^{147}Sm/^{144}Nd	(^{143}Nd/^{144}Nd)$_o$	ϵ Nd$_o$	(^{143}Nd/^{144}Nd)$_I$	ϵ Nd$_I$	^{176}Lu/^{177}Hf	(^{176}Hf/^{177}Hf)$_o$	ϵ Hf$_o$	(^{176}Hf/^{177}Hf)$_I$	ϵ Hf$_I$
0.2026 ± 1	0.512883 ± 40	+4.8 ± 0.8	0.50853 ± 4	+2.4 ± 0.8	0.01806 ± 2	0.282247 ± 43	−21.7 ± 1.5	0.28107 ± 4	+13
					0.01803 ± 4	0.182217 ± 41	−22.8 ± 1.5	0.28104 ± 4	+12.7 ± 1.4

o = at present day; I = at time of crystallization

Data on isotopes in the U, Th-Pb system were presented by Tatsumoto et al. (1972), and Tera and Wasserburg (1974, 1975). The data lie on a discordia: Tatsumoto et al. (1972) determined intersections at 3.3 and 4.65 b.y., but Tera and Wasserburg (1974) preferred 4.42 b.y. with an upper limit of 4.55 b.y. They noted some disagreement with the Tatsumoto et al. (1972) data, especially μ (=^{238}U/^{204}Pb), and discussed their study to determine the effects of leaching during the analytical procedure. Tera and Wasserburg (1974) concluded that 15555 definitely contained radiogenic initial Pb but the data cannot distinguish whether this Pb is from the source of 15555 or a crustal contaminant. The upper discordia intersection may indicate that 15555 was produced from undifferentiated lunar mantle or from one which differentiated rapidly at ~4.42 b.y. This study was

expanded by Tera and Wasserburg (1975) in obtaining an internal U-Pb isochron on 15555. The most critical errors result from ^{204}Pb terrestrial contamination, and isochrons including ^{204}Pb data are not fully convincing. They concluded that 15555 does have an internal isochron in reasonable accord with Rb-Sr and Ar-Ar ages; the ages determined from intersections (cf. slope) are 4.36-4.43 b.y. and 3.19-3.33 b.y. (Fig. 13). Again, the simplest interpretation is of a two-stage development with the source forming at ~4.42 b.y. Nunes et al. (1975) have the opinion that considering the possibilities of 3-stage Pb evolution, a 4.42 b.y. source age is merely conjecture.

U-Pb internal isochron for 15555. If, on the basis of Rb-Sr data a lower intersection at 3.3 AE is chosen then the isochron (passing through the center of total rock point) yields an upper intersection at the magic point 4.42 AE. A best fit line yields 3.26 AE and 4.40 AE respectively for lower and upper intersections.
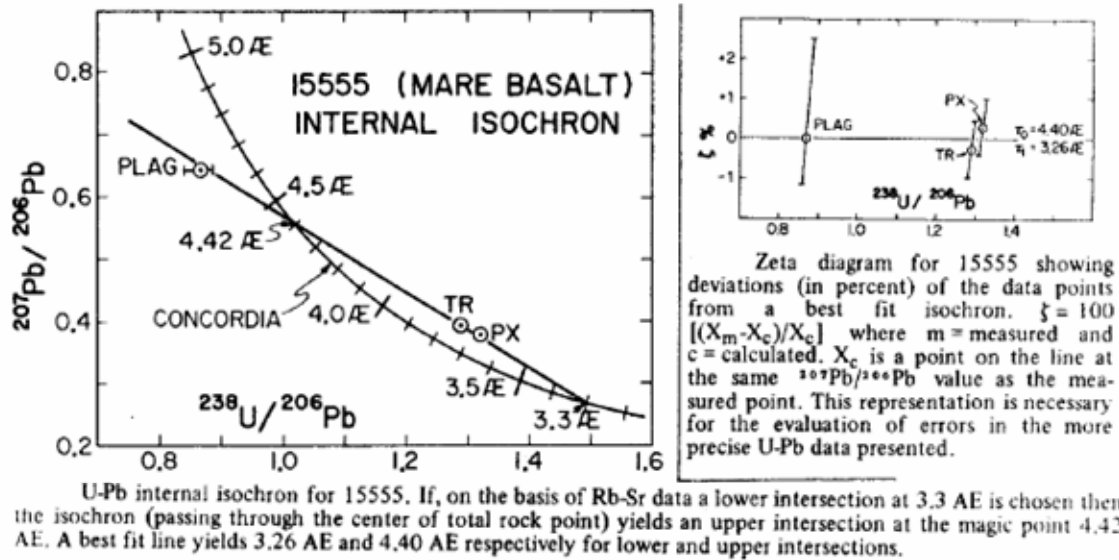
Figure 13. U-Pb internal isochron (Tera and Wasserburg, 1975).

Lightner and Marti (1972) determined a U, Th-He age of 2.8 b.y. (with an assumed U abundance), again suggesting some rare gas loss. Anderson and Hinthorne (1973) determined ^{207}Pb/^{206}Pb ages of 3.36 ± 0.06 b.y. and 3.46 ± 0.09 b.y. from ion microprobe analyses of an Y-Zr phase in 15555, and gave other Pb isotopic data. Rosholt (1974) provided data on the ^{232}Th/^{230}Th activity in a discussion of radioactivity and its sources.

Whole rock Sm-Nd isotopic data were presented by Lugmair (1975) (Table 7a) and discussed by Lugmair and Marti (1977, 1978). 15555 lies on a 4.40 ± 0.06 b.y. isochron with 75075 and 75055, and this was the last time that the sources of these samples had the common parameter of a chondritic Sm/Nd ratio (Not all mare basalts fall on this isochron). The source region for 15555 evolved with positive epsilon until eruption at 3.3 b.y. when light REEs were enriched, reducing Sm/Nd ~3.5% to the present near-chondritic ratio (Lugmair and Marti, 1977, 1978) (Fig. 14). T_{ICE} is very imprecise at 6.18 ± 0.54 b.y. because of this ratio. Whole rock Sm-Nd isotopic data was also presented by Unruh et al. (1984), in addition to whole-rock Lu-Hf data (Table 7b). The whole-rock $\in$Nd ($\in$Ndo in Table 7b) is higher than the quartz-normative basalts 15065 and 15076. The Lu/Hf ratio is less than chondritic, like all mare basalts, thus $\in$Hf has been falling since crystallization.
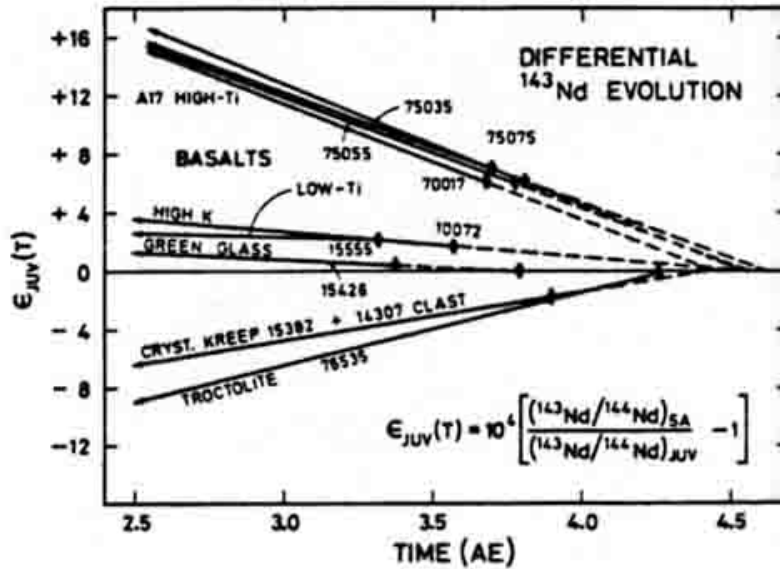
The differential ^{143}Nd evolution $\epsilon_{JUV}(T)$ relative to Juvinas is shown for four Apollo 17 basalts, one each Apollo 11 and 15 basalt, green glass 15426, one each KREEP basalt and clast and troctolite 76535.

Figure 14. Sm evolution (Lugmair and Marti, 1978).

RARE GASES AND EXPOSURE AGES: Exposure ages calculated from rare gas isotopic data are listed in Table 8, and are consistent. Podosek et al. (1972) stated that their 90 m.y. age is an upper limit for excavation from a depth greater than the equivalent of 1000 g/cm^2 burial, and excavation could be more recent from shallower depths. Exposure ages determined from cosmic ray tracks are lower: 34 m.y. (Behrmann et al., 1972); 1 m.y. (suntan) and 26 m.y. (subdecimeter) (Bhandari et al., 1972); maximum 26 ± 5 m.y. (Poupeau et al., 1972); less than 5 m.y. (Fleischer et al., 1973), and presumably indicate that rare gas exposure was at shallow depth rather than actually at the surface.

Apart from the studies listed in Table 8, which present considerable rare gas isotopic data, He, Ne, and Ar isotopes were studied by Megrue (1973) using laser probe mass spectrometry in a search for primordial lunar gases. No unequivocal evidence for such gases exist: Megrue (1973) concluded that He, Ne, and Ar are mainly of solar wind origin (similar to Apollo 12 foil experiment) with some cosmogenic contribution. Data collected from a vug on the surface indicate that vugs may be very efficient collectors of solar wind irradiations. Fireman (1972) investigated ^{37}Ar and ^{39}Ar produced from flares and rays, and attributed the ^{37}Ar/Ca to solar flares in the few years before the mission. Fireman et al. (1972) tabulated information on ^{3}H, ^{37}Ar, and ^{39}Ar at several depths in 15555, again correlated with solar flare activity. Marti and Lightner (1972) found that Ne, ^{36}Ar, and ^{38}Ar are almost purely spallation products; in contrast Kr and Xe have sizeable trapped componee been made to determine exposure ages (above), exposure history, and erosion rates. Behrmann et al. (1972) noted that the depth dependence of

track intensity is flatter than would be expected of a simple exposure history, and that the sample was buried under a few centimeters of soil until recently; solar flare tracks are not observed on the outer part. An upper limit of 1.3 ± 0.1 mm/yr mass wastage erosion is calculated from a comparison of the 26 m.y. track age with the ~85 m.y. rare gas age. Bhandari et al. (1972, 1973) diagrammed the track profile (density/depth) (Fig. 15). Poupeau et al. (1972) determined track densities at the center, midway, and surface of the sample. The latter are more dense and result from solar flares. Fleischer et al. (1973) also determined track densities at various locations within the sample. The study of Fireman (1972) on rare gases was to elucidate the exposure of 15555 to the solar wind.

TABLE 15555-8. Rare gas exposure ages (m.y.) for 15555

REFERENCE	Ar	He	Ne	Kr
Husain (1974) Husain et al. (1972)	80 ± 10 81^a	77^a	73^a	
York et al. (1972a)	$79^b, 72$			
Podosek et al. (1972)	$90^c \pm 10$			
Marti and Lightner (1972)		62		$81 \begin{smallmatrix}+17\\-7\end{smallmatrix}$

Notes:

    (a) unirradiated
    (b) given as 81 in York et al. (1972b)
    (c) plagioclase
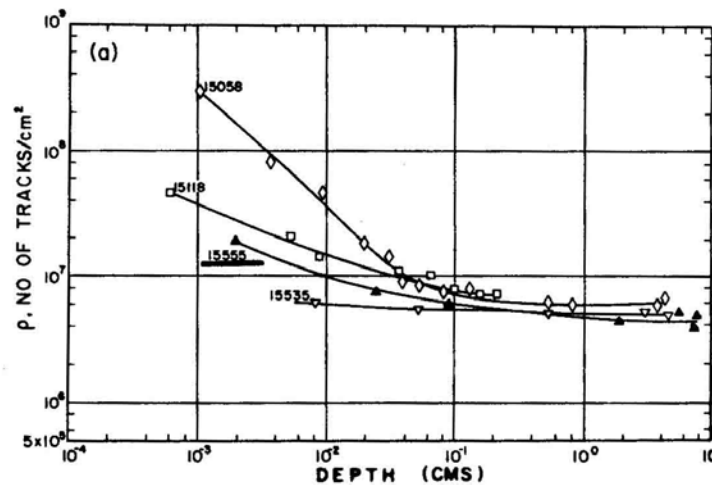
Figure 15. Track density profile (Bhandari et al., 1973).

PHYSICAL PROPERTIES: Basic magnetic measurements and NRM determinations are presented by Collinson et al. (1972, 1973), Pearce et al. (1972, 1973), and Dunn and Fuller (1972). Nagata et al. (1972, 1973) presented basic magnetic data and Hargraves et al. (1972) presented NRM results. The results are in general agreement that 15555 contains little iron; that present is predominantly multidomain and exhibits a very small NRM. Demagnetization curves from different laboratories (Fig. 16) are in good agreement, except that Pearce et al. (1973) found that demagnetization did not yield meaningful data (attributed to multidomain iron grains dominating the sample). The hard NRM is fairly stable, but weaker than other samples of similar age, and scatter probably results from the high noise levels for such weak fields. The direction is roughly constant (Collinson et al., 1972). Nagata et al. (1973) presented a thermomagnetic curve (intensity vs. temperature) (Fig. 17) without specific discussion.
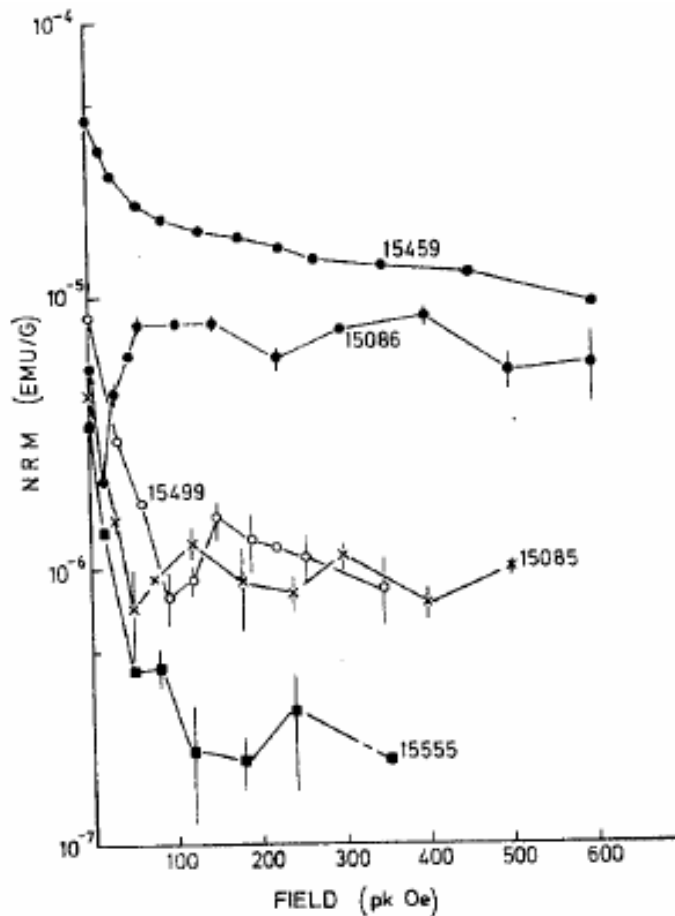
Alternating field demagnetization of Apollo 15 samples. Vertical bars indicate range of intensities obtained after repeated demagnetization.

Fig. 16a
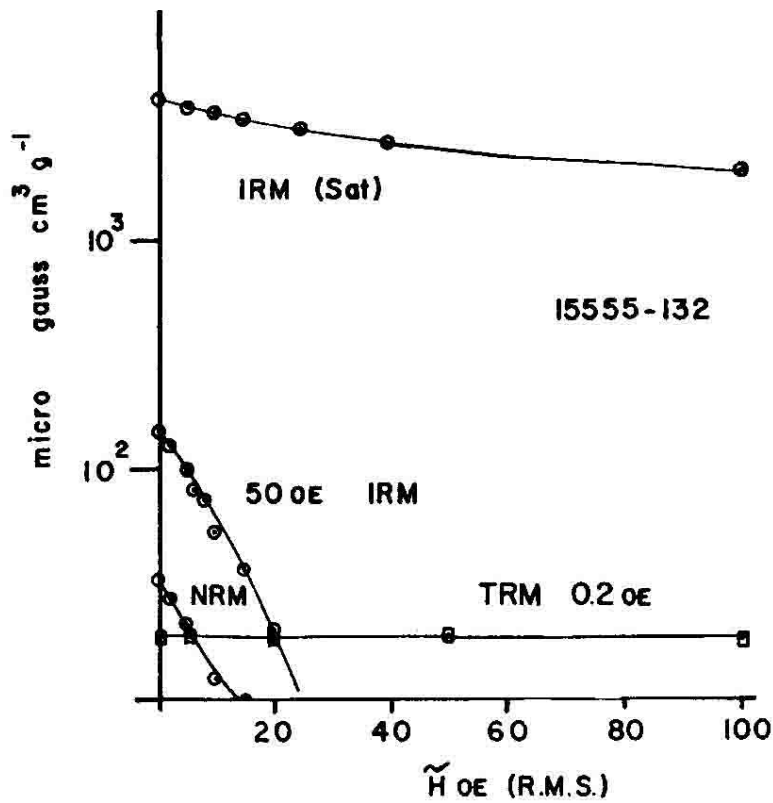
AF demagnetization characteristics of 15555,132.

Fig. 16b
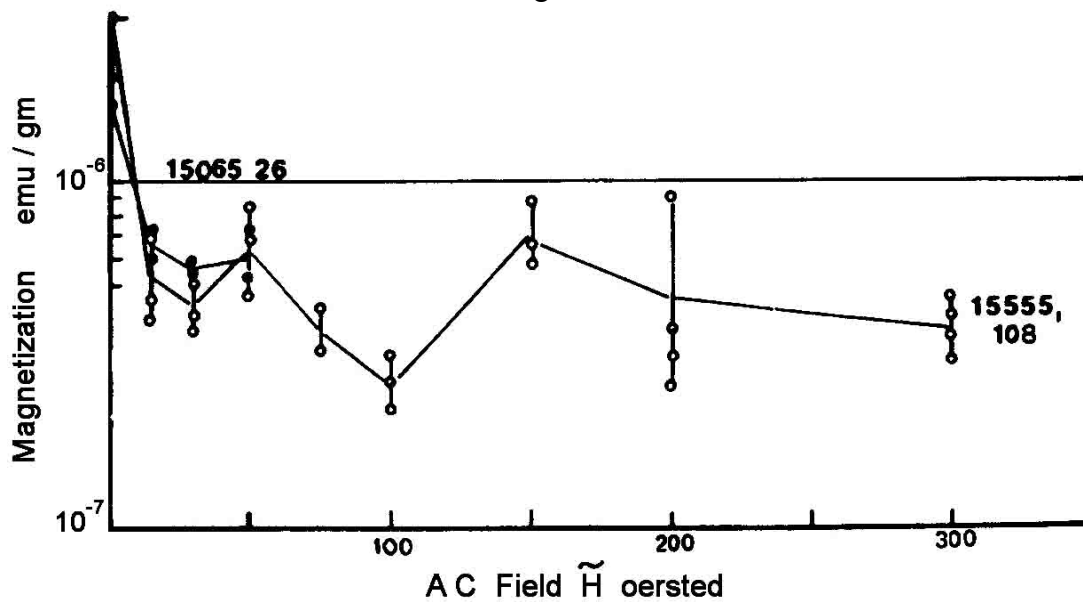
Fig. 16c

Figure 16. AF demagnetization. (a) Collinson et al. (1973);
(b) Dunn and Fuller (1972); (c) Hargraves and Dorety (1972).
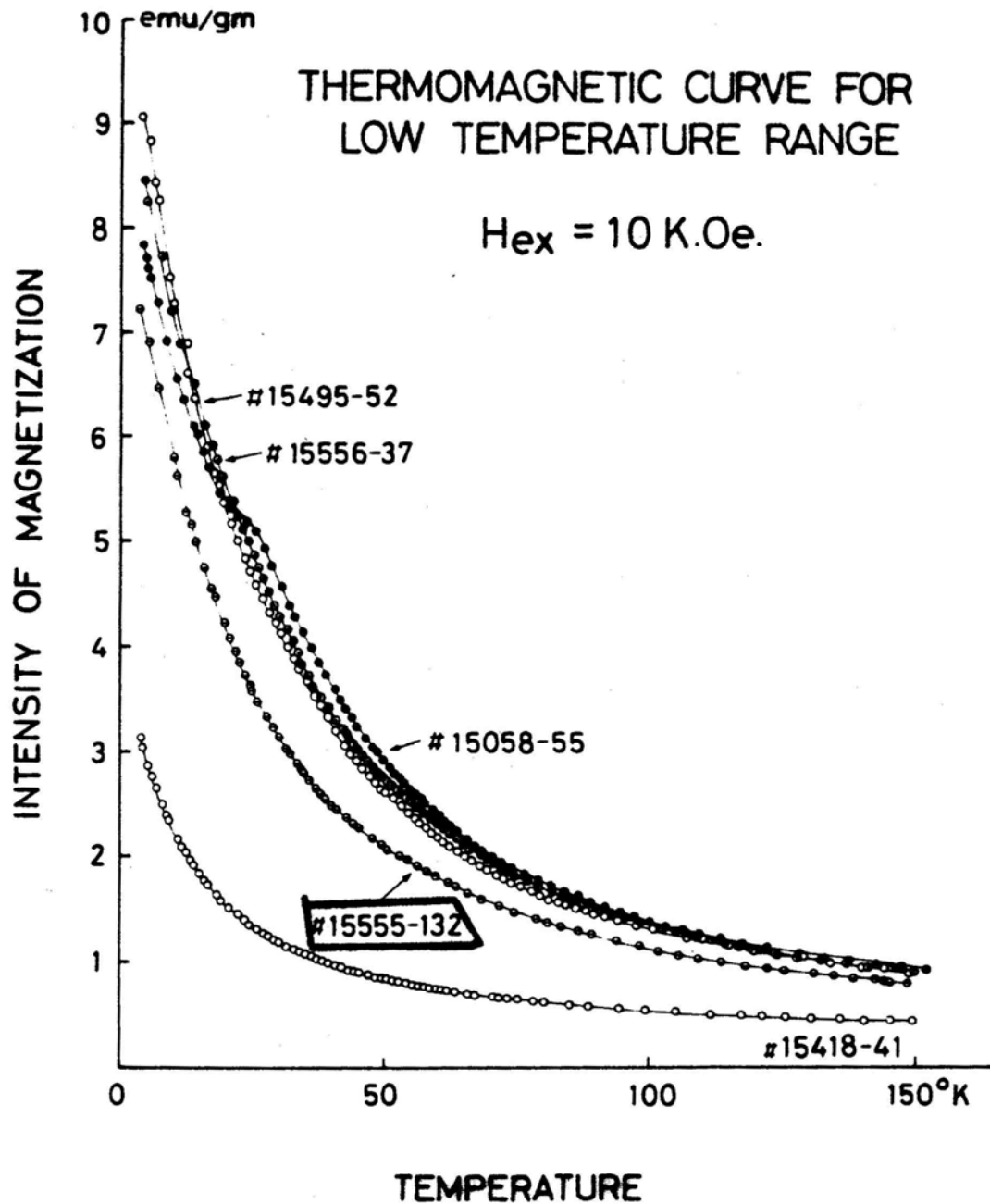
Figure 17. Thermomagnetic curve (Nagata et al., 1973).

Schwerer and Nagata (1976) applied a technique of magnetic granulometry to previously reported data for the temperature dependence of isothermal remanent magnetization. They arrived at the conclusion that, while igneous rocks generally have a larger fraction of metallic iron as fine particles, 15555 is an extreme case in which particles with mean diameters less than 100 Å account for about 88% of the total metallic iron.

Chung and Westphal (1973) tabulated and plotted (Fig. 18) dielectric data without specific discussion, and other electrical conductivity measurements were presented by Schwerer et al. (1973, 1974) for different oxidation-reduction conditions (Fig.19). Schwerer et al. (1973) also presented Mossbauer spectra for an interior portion and surface scrapings taken under oxidizing conditions following a reduction process.
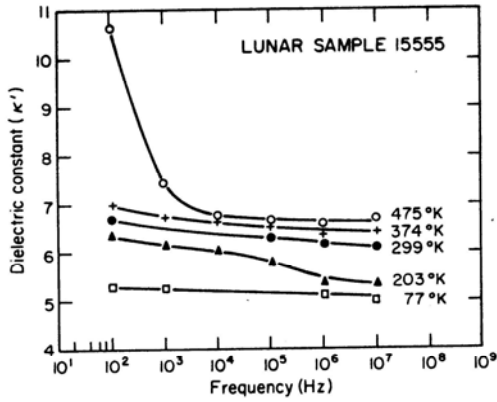

Dielectric constant of sample 15555,88 as a function of frequency and temperature.
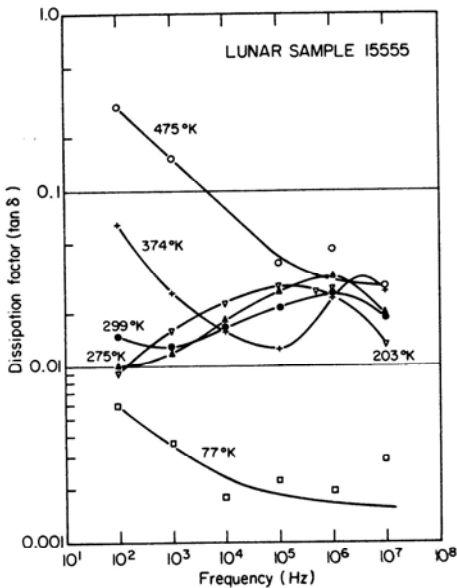
Dielectric losses in sample 15555,88 as a function of frequency and temperature.
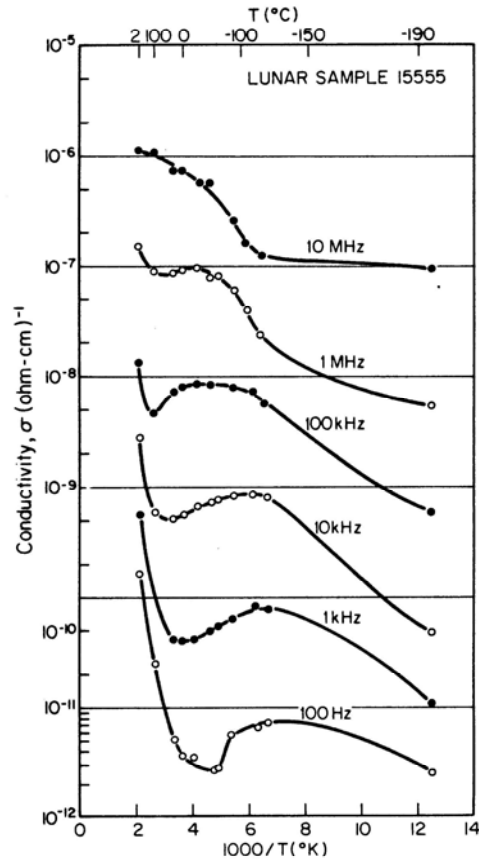
Electrical conductivity of sample 15555,88 as a function of frequency and temperature.

Figure 18. Dielectric spectra (Chung and Westphal, 1973).

Tittmann et al. (1972a,b) found unusually low elastic velocities for 15555: Rayleigh wave (velocity (VR) of 0.28-0.33 km/sec; bulk longitudinal wave velocity (Vp) 0.70-0.95 km/sec. These low velocities result from microfractures, illustrated on an SEM photograph in Tittmann et al. (1972a). Warren et al. (1973) also measured acoustic velocities under uniaxial loading (Fig. 20), also demonstrating low values. They also measured the internal friction (Q) on a glass of 15555 composition. Chung (1973)determined elastic wave velocities under confining pressures from 0.5 to 7 kb (Fig. 21, Table 9), under which pressures the acoustic velocities are similar to those of other rocks.
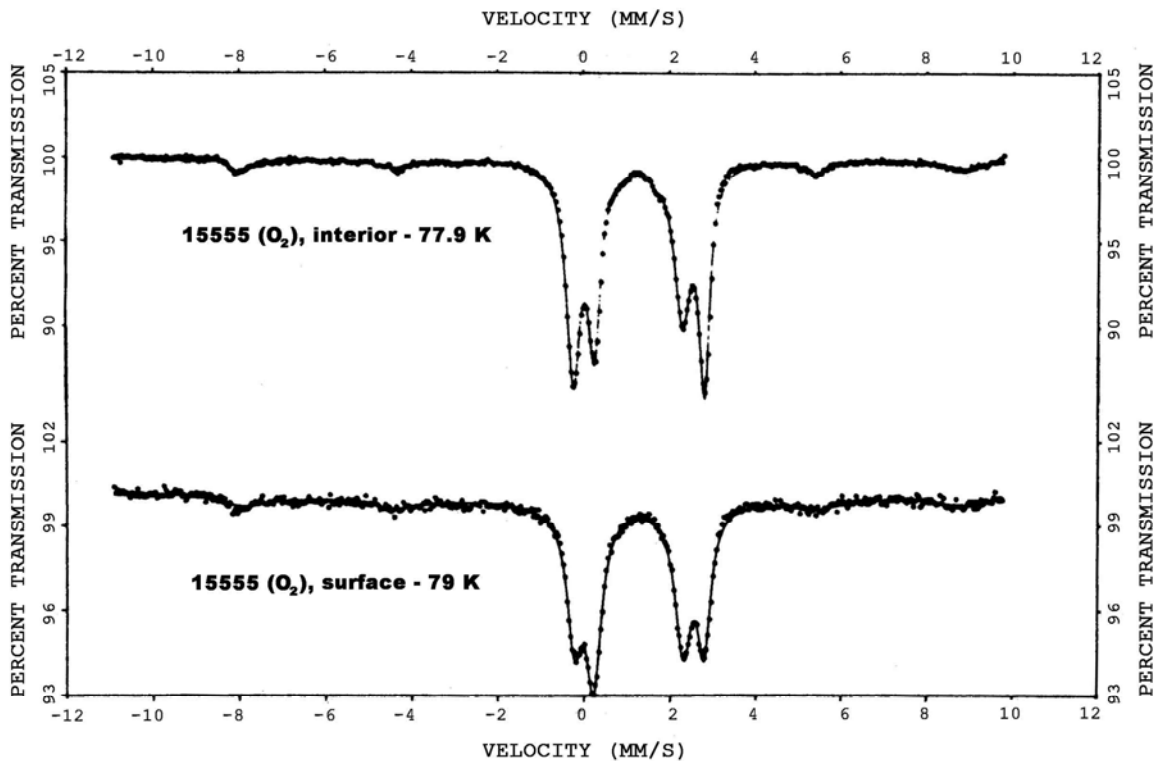
Mössbauer spectra of an interior portion and surface scrapings of Apollo sample
15555 after annealing at 800°C first in He–H₂, then in He–O₂.

Fig. 19a

CONDUCTIVITY,
(ohm-cm)$^{-1}$

TEMPERATURE C
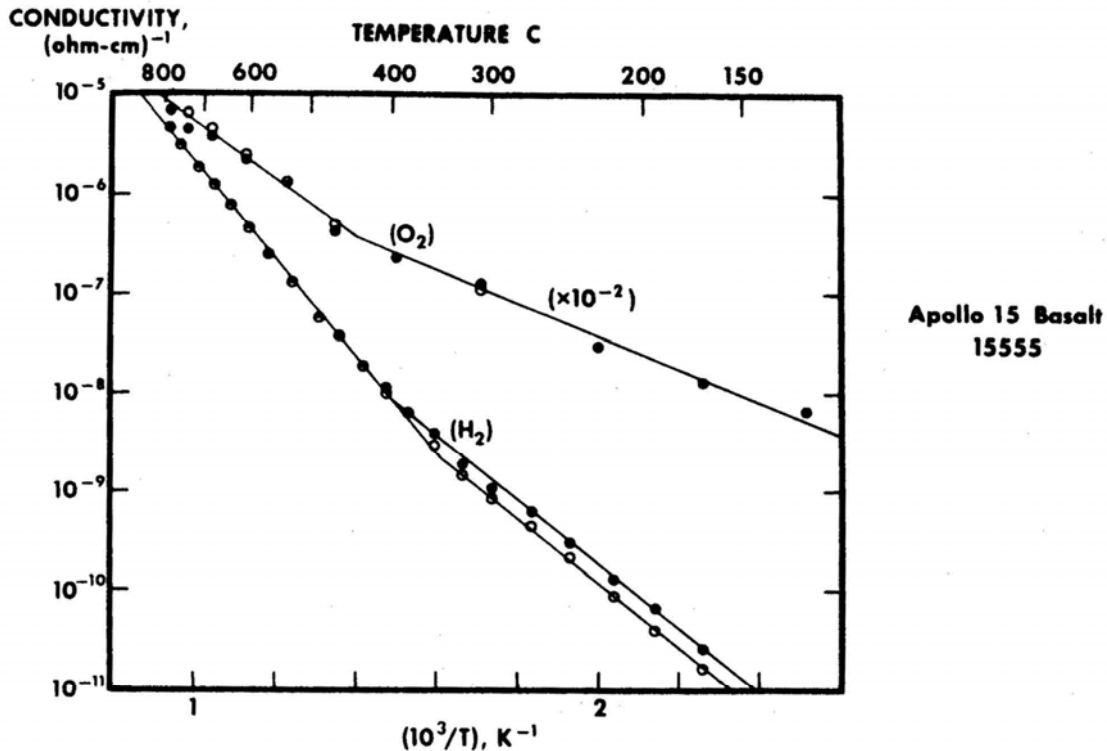
Electrical conductivity (dc, full symbols; ac, open symbols) for lunar basalt (Apollo 15555) in reducing and oxidizing atmospheres (lower and upper sets of curves, respectively). Solid lines are results of least-squares fit to Equation 1. (For purposes of presentation, data for the oxidizing environment have been reduced by a factor of 100.)

Fig. 19b

Figure 19. (a) Mossbauer spectra and
(b) electrical conductivity (Schwerer et al., 1974).

Hemingway et al. (1973) tabulated and plotted specific heat determinations over a temperature range of 83.56°K to 363.53°K (Table 10). The data are similar to those for other lunar rocks and soils.

Adams and McCord (1972) and Charrette and Adams (1975) presented reflection spectra for 15555, and Brito et al. (1973) made thermoluminescence studies on six samples from the center to the outside.

Cukiermann and Uhlmann (1974) studied the viscous flow behavior of a 15555-like composition glass at 620° to 700°C and 1215° to 1400°C under mildly reducing conditions. They also studied the effect of oxidation state on viscosity, finding that a decrease in Fe^{2+}/Fe^{3+} produced a dramatic increase in viscosity.
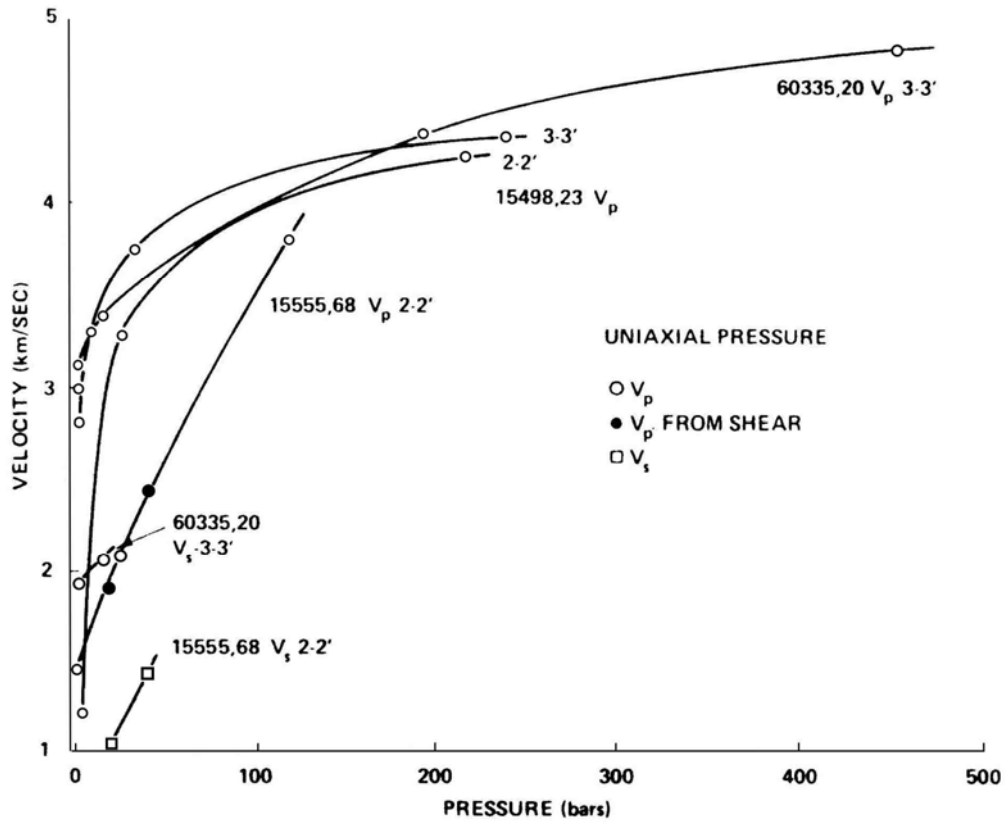
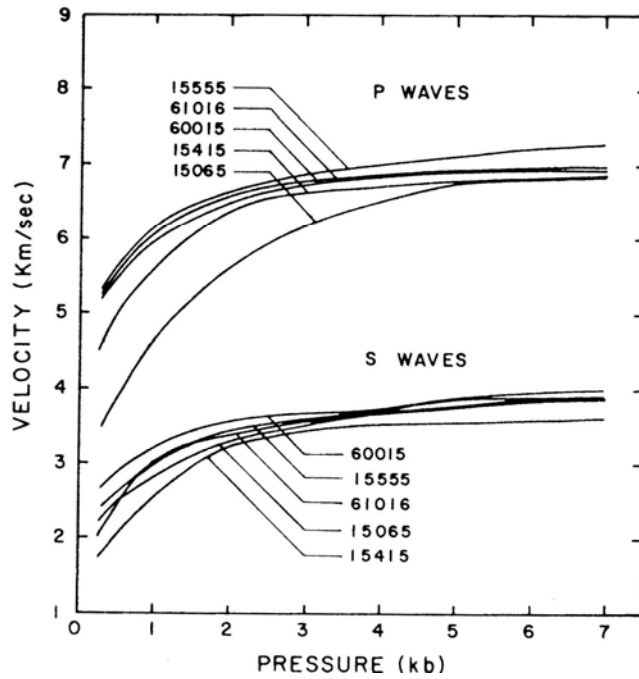Figure 20. Seismic velocity as a function of pressure (Warren et al., 1973).

Figure 21. Seismic velocity as a function of pressure (Chung, 1973) .

TABLE 15555-9. Elastic wave velocities for 15555
(Chung, 1973)

| | Pressure, kb | | | | | | | | |
	0.5	1.0	1.5	2.0	3.0	4.0	5.0	6.0	7.0
P (km/sec)	5.6	6.1	6.45	6.66	6.90	7.02	7.14	7.25	7.30
S (km/sec)	2.6	3.0	3.24	3.45	3.66	3.76	3.87	3.94	4.01

TABLE 15555-10. Specific heat measurements for 15555
(Hemingway et al., 1973).

Temperature °K	Specific heat J/(gram · K)	Temperature °K	Specific heat J/(gram · K)	Temperature °K	Specific heat J/(gram · K)
83.56	0.2088	187.06	0.5180	293.09	0.7556
94.05	0.2414	197.83	0.5456	303.77	0.7703
103.71	0.2715	208.68	0.5736	313.96	0.7895
113.58	0.3038	218.95	0.5983	323.97	0.8071
124.82	0.3389	230.05	0.6230	333.68	0.8222
136.51	0.3749	240.98	0.6481	343.36	0.8397
143.07	0.3946	249.20	0.6648	353.28	0.8565
154.35	0.4276	260.22	0.6874	363.53	0.8728
165.24	0.4586	271.21	0.7084		
176.18	0.4879	281.80	0.7330		

Cukiermann et al. (1973) also reported data on the viscosity of a similar glass sample, as well as on the crystallization kinetics; 15555 does not easily form a glass.

PROCESSING AND SUBDIVISIONS: 15555 has been widely split, including the production of sawn slabs, resulting in about 800 subsamples. Several allocations were made from undocumented chips loose in the sample container. The basic subdivisions are shown in Figure 22. Nearly all the thin sections are from subdivisions of slab ,57, with the exceptions of several made from ,14, an undocumented loose fragment (Fig. 23). The large pieces ,47 (3654 g) and ,56 (2226 g) are still intact. ,58 has been subdivided into numerous subsamples, many of which are 100-300 g. A large proportion of these are now PAO samples.
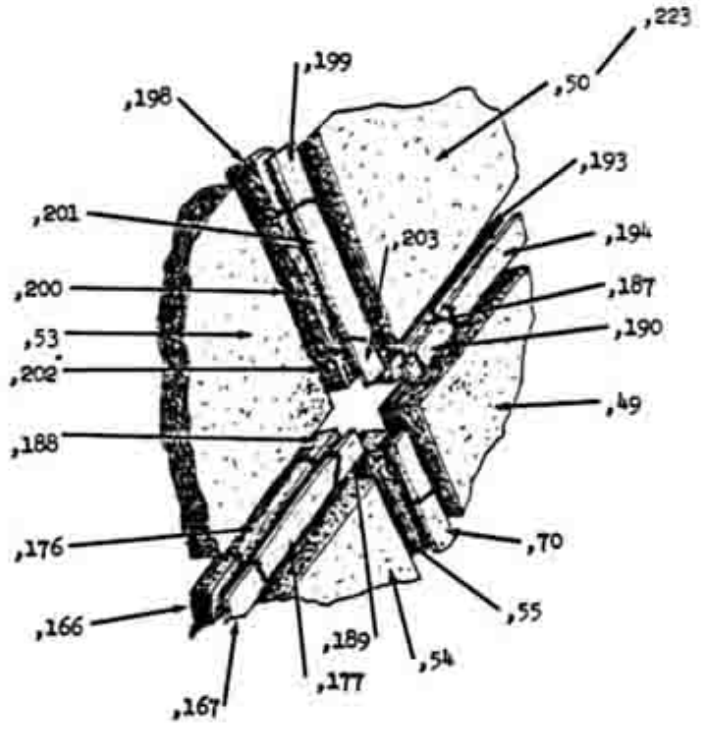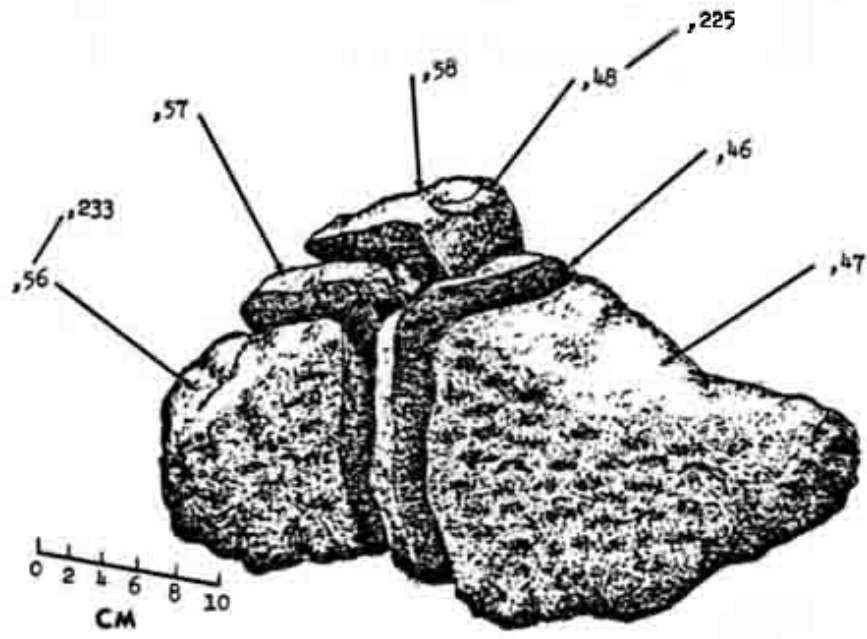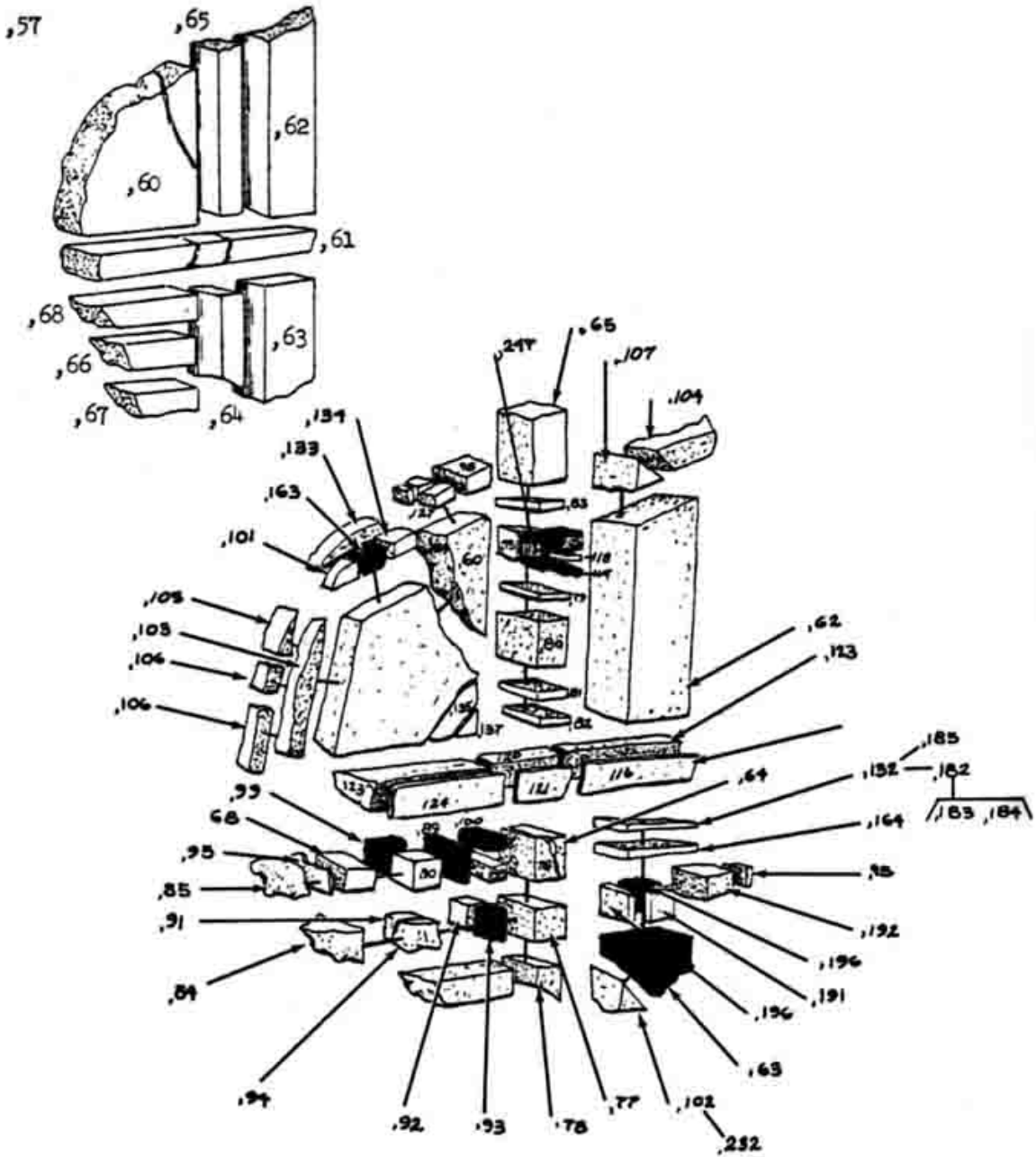
Figure 22. Main subdivision of 15555.

Figure 23. Subdivision of slab 1555,57.